Journal of Aircraft, Volume 61, Issue 2, March 2024, pp. 485-502
DOI: 10.2514/1.C037194

Toward Estimating Noise–Power–Distance Curves for Propeller-Powered Zero-Emission Hydrogen Aircraft

Daniel C. Amargianitakis* and Rodney H. Self†
University of Southampton, Southampton, England SO17 1BJ, United Kingdom
Antonio J. Torija‡
University of Salford, Manchester, England M5 4WT, United Kingdom
Anderson R. Proença§
Cranfield University, Cranfield, England MK43 0AL, United Kingdom
and
Athanasios P. Synodinos¶
University of Southampton, Southampton, England SO17 1BJ, United Kingdom

https://doi.org/10.2514/1.C037194

As part of the UK Research and Innovation project New Aviation, Propulsion, Knowledge and Innovation Network (NAPKIN), a high-level framework was developed for the assessment of the noise impact of the proposed regional-sized hydrogen-powered aircraft. This study consists of the methodology used to generate the industry-standard noise–power–distance (NPD) curves from individual component noise analysis, specifically propeller tonal noise. The model is based on an asymptotic analysis of a frequency domain propeller tonal noise model combined with a linear approximation, taking advantage of the logarithmic nature of noise. An error analysis on the linear approximation assumption proves that the relative error between predicted and actual values of the noise remains below 10% for appropriately chosen baseline points. Verification of the framework was achieved through a bench-marking procedure that compared predictions of departure NPD curves for current technology regional aircraft against published ones over a range of operational power settings. Finally, departure and approach NPD predictions for three of the NAPKIN hydrogen concept aircraft are presented. Concepts featuring a larger, slower-rotating propeller with an increased number of blades relative to the reference aircraft showed benefits over the reference aircraft, despite, in some cases, increases in maximum takeoff weight.

Nomenclature

B	=	number of blades
$\bar{C}_L$, $\bar{C}_D$	=	average section lift and drag coefficients
c_0	=	ambient speed of sound, $\mathrm{m} \cdot \mathrm{s}^{-1}$
D	=	propeller diameter, m
d	=	slant distance, m
F_1	=	spectral shape function
J_{mB}	=	Bessel function of order mB
k_x and k_y	=	axial and radial wavenumbers
L_{f_1}	=	sound pressure level of fundamental tone, dB
L_p	=	sound pressure level, dB
M_h	=	helicoidal (advance) tip Mach number, $\sqrt{M_T^2 + M_x^2}$
M_r	=	blade section Mach number, $\sqrt{z^2 M_T^2 + M_x^2}$
M_t	=	tip rotational Mach number, $\Omega R_t / c_0$
M_x	=	flight Mach number, V/c_0
m	=	harmonic of blade passing frequency
N	=	rotational frequency, rpm
P_{mB}	=	complex Fourier coefficient of p
p	=	sound pressure, Pa
R	=	distance between observer and propeller, m
R_t	=	propeller radius, m
$\bar{t}_b$	=	average maximum thickness-to-chord ratio
W	=	sound power, W
Δ	=	indicates change in noise level, dB
(θ, φ)	=	spherical coordinate emission angles
ρ_0	=	density of the fluid, $\mathrm{kg} \cdot \mathrm{m}^{-3}$
Ψ_D, Ψ_L, and Ψ_V	=	transforms of drag, lift, and thickness source terms

Received 1 September 2022; revision received 20 August 2023; accepted for publication 30 September 2023; published online 13 December 2023. Copyright © 2023 by Daniel Constantinos Amargianitakis, Rodney Self, Antonio Torija Martinez, and Anderson. Published by the American Institute of Aeronautics and Astronautics, Inc., with permission. All requests for copying and permission to reprint should be submitted to CCC at www.copyright.com; employ the eISSN 1533-3868 to initiate your request. See also AIAA Rights and Permissions www.aiaa.org/randp.

*Ph.D. Student, Institute of Sound and Vibration Research, Hampshire; dca1g14@soton.ac.uk (Corresponding Author).
†Professor, Institute of Sound and Vibration Research, Hampshire.
‡Reader (Associate Professor), Acoustical Engineering, Acoustics Research Centre.
§Lecturer in Aerodynamics, Applied Aerodynamics Group, School of Aerospace, Bedford.
¶Visiting Academic, Institute of Sound and Vibration Research, Hampshire.

I. Introduction

AIMING at transitioning to a future zero-emission aviation network within the United Kingdom, the UK Research and Innovation (UKRI) government agency has funded a series of research and development projects across all aspects of flight. From small fully electric unmanned aerial vehicles (UAVs) capable of autonomous cargo delivery, the advancement of electrification technologies in aviation, and the development of advanced air mobility (AAM) transport networks based on large electric vertical takeoff and landing (eVTOL) vehicles, all the way to low- and zero-carbon domestic and short-haul aviation, the UKRI grants cover a wide gamut of activities.

In the regional and subregional classes of aircraft, concepts leverage technologies such as direct hydrogen combustion turbo-gas engines or combinations of hydrogen fuel cells and electric motors as means of energy storage and delivery systems to meet the zero-emission goals. These propulsion architectures are most commonly coupled with propellers or ducted fans as a means of thrust generation. In the absence of turbomachinery and reciprocating engines, the propeller becomes the main noise-generating mechanism.

The assessment of noise emissions at the conceptual and preliminary design stages of novel aircraft requires high-level tools designed for significantly reduced data and input requirements. Such tools provide i) critical information to manufacturers about how design

Published by AIAA. This is the Author Accepted Manuscript issued with: Creative Commons Attribution License (CC:BY 4.0).
The final published version (version of record) is available online at DOI:10.2514/1.C037194. Please refer to any applicable publisher terms of use.

decisions impact the individual noise-generating mechanisms and inform the exploration of large design spaces with additional acoustical data; ii) inform airports and airlines of the impact the introduction of concept aircraft will have on fleet noise emissions; and iii) contribute to assessing future noise exposure contours around airports to help minimize the effect on communities surrounding airports. The ability to quantify the effects of changes in design parameters on the propeller noise and, consequently, the entire aircraft while retaining minimal input data and computation requirements will allow for a larger design space to be explored.

An existing framework has been extended for the construction of purely computational noise–power–distance (NPD) curves for aircraft dominated by propeller harmonic noise. The original framework is based on work by Synodinos et al. [1] for conventional fixed-wing airliners. At the foundation of the model lies a lumped noise source representative of the whole air vehicle's noise emissions. The lumped source is composed of the individual noise-generating mechanisms that contribute to the air vehicle's overall noise signature. This allows for lumped sources to be built and applied on a case-by-case basis, depending on the relevant/dominant noise sources.

The framework is based on the knowledge of the baseline absolute noise levels of an appropriately chosen reference aircraft. The changes in relative levels, due to technological design and operational changes, of the individual noise sources are calculated by scaling laws derived by analytical or semi-empirical prediction models for each source, respectively. Once all source levels are combined, the lumped source is defined by an overall sound power level (PWL), a directivity factor and a normalized spectral shape. The lumped source is then used in the simulated flyover procedure defined by European Civil Aviation Conference (ECAC) Doc29 [2] and the Society of Automotive Engineers—Aerospace Information Report (SAE-AIR) 1845 [3,4] computational method. Sound propagation and atmospheric attenuation are also handled as suggested by Doc29 using SAE-ARP 866A [5].

Evaluation of community noise may then be carried out through the assessment of noise exposure footprints and contours generated through conventional grid-point airport noise tools such as the Federal Aviation Administration's (FAA's) Aviation Environmental Design Tool (AEDT) [6] and Eurocontrol's tool IMPACT [7] or high-level community noise models such as Rapid Aviation Noise Evaluator (RANE) [8]. All these tools use NPD data as standard input.

Specifically, the work herein contributes two key components: i) modifications to the framework to accept changes in noise levels of tonal noise sources due to changes in the harmonic spectral shapes of individual sources, and ii) a model for computing such changes in harmonic spectral content for propeller steady tonal noise. It is worth mentioning that the modifications allow for any tonal source to be treated identically, allowing for future applications of the framework dealing with, for example, turbomachinery noise or cavity resonance. As this study is focused on propeller harmonic noise, the model derived provides the required changes in spectral noise levels (deltas) between the reference and concept aircraft as inputs to the framework.

Benchmarking of the model was performed using four current propeller-powered aircraft. The aircraft were chosen to cover a wide range of propeller design and operation points. Finally, to demonstrate the capability of the model, predictions for three hydrogen-powered aircraft concepts are generated and discussed. The concepts were developed as a part of project New Aviation, Propulsion, Knowledge and Innovation Network (NAPKIN).

II. Background

Whole aircraft noise models are typically characterized by three components: i) noise source definition, ii) noise propagation, and iii) trajectory/operation modeling. Noise source definition attempts to capture and combine all individual noise-generating mechanisms onboard and in air vehicles, quantifying them through their overall acoustic sound power contribution, spectral content, and directivity across various power settings. Depending on the nature and difficulty of predicting individual sources, methods to estimate them vary from analytical to numerical and calibrated semi-empirical methods. Subsequently, the noise levels generated are propagated to observer locations using appropriate models, taking into account spherical spreading and atmospheric absorption/turbulence (other effects may be modeled depending on the fidelity required). Finally, as the noise impact of the vehicles in flight is of interest, appropriate modeling of the vehicle's trajectory is necessary. This accounts for the location and orientation of the aircraft in space as a function of time, as well as air vehicles and propulsion system performance.

The NPD process standardizes the way of correlating air-vehicle source noise and operation. Traditionally, NPD curves are the result of expensive experimental campaigns during the noise certification process of an aircraft. This impedes the understanding of the certification and operational noise of novel aircraft due to the lack of flight-capable prototypes and the resulting measured data. Models for computationally predicting NPD curves (from source definition to operation) provide crucial insight into the overall impact of implementing new technologies or introducing new aircraft (and their operations) to the already existing aviation environment. A few examples of whole air-vehicle noise models are NASA ANOPP2 [9] and the DLR (German Aerospace Center) Parametric Aircraft Noise Analysis Module (PANAM) tool [10,11]. Recent work by Rizzi et al. [12–16] has demonstrated the entire process of computationally generating NPD curves for novel (AAM) aircraft and incorporating them into AEDT for the assessment of community noise exposure, while a similar approach is taken for novel aircraft using physics-based models (PBM) by research groups at Georgia Institute of Technology and Purdue University [17] (FAA Ascent Project 43), including work on novel supersonic aircraft.

Finally, beyond noise type certification, NPD curves are used in airport/community noise impact studies. The study of community noise exposure revolves around the generation of noise exposure contour maps for individual aircraft performing single operations as well as aircraft fleet operations. These maps are important to legislators, certification bodies, and airport management committees as they provide a graphical and comprehensible means of describing the acoustic impact of aircraft movements around airports and densely populated areas. The industry standard for generating them is presented by the methods of ECAC Doc 29 [2] and International Civil Aviation Organization (ICAO) Doc 9911 [18], adopted by software such as the Federal Aviation Administration (FAA) AEDT. The principal noise input requires NPD curves. Other airport noise models also adopt NPD curves as a method for noise input. European tools that implement grid-point methodology are Eurocontrol's IMPACT [7] and STAPES (SysTem for AirPort noise Exposure Studies), and the UK CAA's Aircraft Noise Contour 2 (ANCON2) [19] based on the original ANCON (a tool developed and used by the UK Civil Aviation Authority) model.

III. Methodology

A. Overview

An overview of the methodology used to generate the NPD curves for propeller-powered aircraft follows: Figure 1 shows a flow diagram describing the various aspects of the framework and identifying the two key components previously mentioned. Initially, a representative baseline aircraft is chosen. This baseline matches the operation, design, and technology levels of the concept as best as possible. Synodinos [20] showed that, for fixed-wing turbofan engines, predecessor aircraft form the best baseline aircraft. The baseline aircraft provides absolute noise level data representative of the whole aircraft (NPD data) and individual source baseline data.

The concept air vehicle is then represented as a series of changes (deltas) relative to baseline aircraft from both operational perspective and design. Changes in noise levels (ΔL) are calculated using individual noise source methods and applied to the baseline levels, before being combined to form the lumped source representation of the novel aircraft. The lumped noise source is then computationally flown a prescribed flight path, while noise levels at an observer location are calculated to form a time history for that particular flight

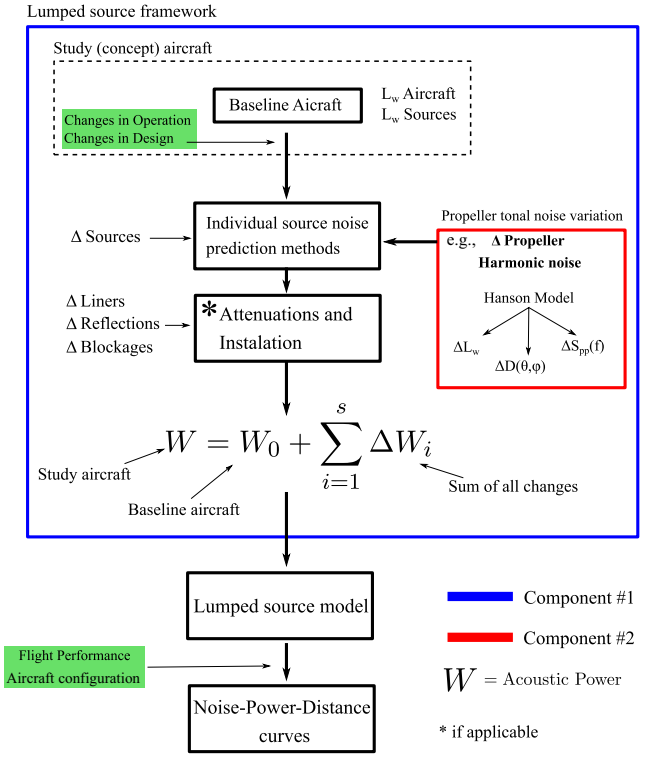

Fig. 1 Flow diagram of the lumped noise source modeling framework.

event. The event time history is used to calculate event metrics such as $L_{A,\max}$ and sound exposure level (SEL).

B. Lumped Source Model: Working with Changes in Noise, ΔPWL

Consider a baseline aircraft, which is made up of noise sources emitting a total sound power of W_0. The total sound power W, of a concept, is then given as a function of the baseline and the individual noise source changes ΔW_i, which are a direct result of operational or technological changes:

$$W = W_0 + \sum_{i=1}^{s} \Delta W_i \tag{1}$$

where i indexes through the total number of sources s. It is worth noting that $\Delta W_i = W_i$ for noise sources that did not exist before and that $\Delta W_i = -W_i$ for sources that were no longer present.

The basic definition of a lumped noise source model in terms of a sound pressure level (SPL) is given in Eq. (2).

$$L_p(\theta,\varphi,r) = 10\log\left[\frac{WD(\theta,\varphi)\bar{S}_{pp}(f)}{r^2}C\right] \tag{2}$$

where θ and φ are the emission polar and azimuthal angles (Fig. 3), r is the distance between the lumped source location and the observer of interest, D is directivity factor normalized to possess unit power, as is the power spectral density $\bar{S}_{pp}$, and finally, constant $C = \rho_0 c_0/(4\pi p_{\text{ref}}^2)$.

1. *Variation in Tonal Content*

The changes to the overall sound power manifest through changes to the distribution of energy across frequencies and emission angles between the baseline and the novel air vehicle. Specifically, changes in tonal sources' level and frequency need to be applied to the baseline air-vehicle spectrum.

Consider a case where modifications to a baseline aircraft are made. The baseline aircraft is defined by i) a single $L_{A,\max}$ noise level retrieved from publicly available NPD data [21]; ii) an unweighted 1/3rd octave frequency spectrum of the baseline aircraft during the same operation (this is also available in databases such as the Eurocontrol aircraft noise and performance [ANP]); and iii) relative dominance of the individual sources making up the total aircraft given in terms of average dB levels [22]. The source breakdown methodology is described by Synodinos et al. [1].

The baseline $L_{A,\max}$ is backpropagated to the source, in the form of a 1/3rd octave frequency spectrum. The frequency spectrum of the novel aircraft is calculated by applying deltas across those bands. These deltas, for a tonal source, are the result of changes in the harmonic distribution, such as the specific example of propeller loading and thickness noise, and are implemented as follows:

Propeller discrete tone noise can be represented as the energy sum of all harmonics. Some spectra shape function can be used to tie the distinct harmonic levels to the fundamental tone, allowing the SPL to be represented as

$$L_{p,0} = 10\log_{10}\left(\sum_{f}^{\infty} 10^{\left[L_{f_1,0}+F_1\left(\frac{f}{f_{1,0}}\right)\right]/10}\right) \text{ [dB]} \tag{3}$$

where m is the harmonic number; $f = mB\Omega$ and $f_1 = B\Omega$ represent the frequency of mode m and the fundamental tone, respectively; while $L_{f_1,0}$ is the SPL of the baseline fundamental. F_1 denotes the spectra shape function.

When modifications in terms of operational and/or design parameters are made, changes to the fundamental tone ΔL_{f_1} and the shape of the harmonics ΔF_1 are observed, leaving the new SPL as

$$L_p = 10\log_{10}\left(\sum_{f}^{\infty} 10^{\left[L_{f_1,0}+F_1\left(\frac{f}{f_{1,0}}\right)+\Delta L_{f_1}+\Delta F_1\left(\frac{f}{f_1}\right)\right]/10}\right) \tag{4}$$

where $L_{f_1} = L_{f_1,0} + \Delta L_{f_1}$ represents the new level of the fundamental tone, and $L_m(f) = L_{f_1} + \Delta F_1(f/f_1)$ represents the new sound level of the harmonics. Equation (4) is the SPL equivalent relationship to Eq. (1), accounting not only for changes in the overall sound power but also how the distribution of power changes across the frequency spectrum.

The change in the level of the fundamental frequency ΔL_{f_1} from Eq. (4) may be estimated by

$$\Delta L_{f_1} = 10\log_{10}\left(\frac{p_{f_1}^2}{p_{f_1,0}^2}\right) \tag{5}$$

The average intensity radiated over angles θ and φ, which can be calculated in the far field using the root mean square, may thus be used to determine the system's overall sound power output:

$$W = 4\pi R^2 \bar{I} = \frac{4\pi R^2}{\rho_0 c_0}\int_0^{2\pi}\int_0^{\pi} p_{\text{rms}}^2 R^2 \sin\theta \, \mathrm{d}\theta \, \mathrm{d}\varphi \tag{6}$$

Integration across the spherical surface surrounding the source is required to get the mean acoustic intensity $\bar{I}$. The propeller axis acts as a symmetry axis; therefore, the only dependence of noise on observer location occurs over the polar angle θ. Integration over φ takes a trivial solution.

C. Propeller Tonal Noise Variation

One particular noise source of interest is propeller steady harmonic noise. To generate the required input to the proposed framework, an asymptotic analysis of the frequency domain Hanson model [23] is performed, in order to help quantify how the acoustic energy output of the source varies as a function of changes in the parameters that it is influenced by.

1. *Hanson Model Overview*

Let the propeller of interest be of diameter D (and radius r_t) and number of blades B. The chord-to-diameter ratio is given by B_D, while

the maximum thickness-to-chord ratio by t_b. The propeller is assumed to be in flight with a representative axial Mach number of M_x.

The propeller is rotating at an angular rate of Ω, giving the propeller tip Mach number as M_t. Due to the forward and rotational motion, each blade section sees a relative Mach number of $M_r = \sqrt{M_x^2 + z^2 M_t^2}$, where $z = r_0/r_t$ is the normalized radial coordinate. The loading characteristics are defined in terms of the aerodynamic coefficients C_L and C_D, returning the dimensional force per unit spanwise length (newton/meter) when multiplied by $1/2\rho_0 c_0^2 M_r^2$. The location of the observer is given by the polar angle θ in the plane perpendicular to the propeller plane, while the distance between the center of the propeller hub and the observer is given by r. A detailed illustration of the reference frame can be seen in Fig. 2. Forward flight effects are accounted for through amplitude and frequency shift correction relative to stationary observers [23]. The quadrupole factors are ignored since their contributions in the subsonic regime are negligible [24]. The noise harmonics are given in terms of their Fourier transform coefficients P_{Vm}, P_{Dm}, and P_{Lm} for the thickness, drag, and lift sources, respectively.

The blade passing frequency (BPF) is given by the product of the number of blades, B, of the propeller times its rotation frequency f. The integer multiples of the BPF give the harmonics (or modes) of the propeller sound field. The mth harmonic is therefore given by $mB\Omega$ in terms of the angular rotation rate Ω.

$$\begin{Bmatrix} P_{Vm} \\ P_{Dm} \\ P_{Lm} \end{Bmatrix} = -\frac{\rho_0 c_0^2 B \sin\theta \exp\left[imB\left(\frac{\Omega r}{c_0} - \frac{\pi}{2}\right)\right]}{8\pi(y/D)(1 - M_x \cos\theta)} \int_0^1 M_r^2 \exp(i\phi_s) J_{mB} \times \left(\frac{mBzM_t \sin\theta}{1 - M_x \cos\theta}\right) \begin{Bmatrix} k_x^2 t_b \Psi_V(k_x) \\ ik_x (C_D/2) \Psi_D(k_x) \\ ik_y (C_L/2) \Psi_L(k_x) \end{Bmatrix} \mathrm{d}z \tag{7}$$

where c_0 and ρ_0 are the ambient speed of sound and air density, and ϕ_s represents a phase lag due to blade sweep (neglected further on in this study as simple blade geometry is assumed). The mode number is m, giving the harmonics as multiples of the BPF, $\Omega B/2\pi = N \times B/60$, where N is the revolutions per minute. The nondimensional wave numbers k_x and k_y are defined by

$$k_x = \frac{2mBB_D M_t}{M_r(1 - M_x \cos\theta)} \tag{8}$$

$$k_y = \frac{2mBB_D}{zM_r} \left(\frac{M_x - M_r^2 \cos\theta}{1 - M_x \cos\theta}\right) \tag{9}$$

where angle θ is the polar angle measured from the propeller axis to the observer position vector, as in Fig. 2, and B_D is the ratio of the chord b to the propeller diameter D. The integral form of Eq. (7) proves a simple intuitive connection between the radiated sound and the parameters that influence it.

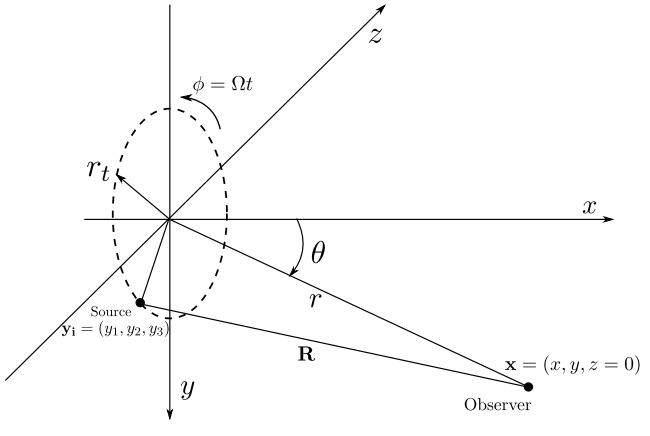

Fig. 2 The acoustic field and the rotating source's geometry.

Ψ_V, Ψ_D, and Ψ_L are the Fourier transforms of the three sources, which are functions of the blade thickness $H(x)$ and loading chordwise distributions $f_D(x)$ and $f_L(x)$:

$$\begin{Bmatrix} \Psi_V(k_x) \\ \Psi_D(k_x) \\ \Psi_L(k_x) \end{Bmatrix} = \int_{-(1/2)}^{1/2} \begin{Bmatrix} H(x) \\ f_D(x) \\ f_L(x) \end{Bmatrix} \exp(ik_x x)\, \mathrm{d}x \tag{10}$$

The "thin-blade" model simplifies the problem; however, it leads to errors in the estimation the higher harmonics of the BPF. Observer locations far from the plane of rotation, $\cos\theta \neq 0$, also experience accuracy reduction. Finally, the model includes Doppler correction components in both amplitude and frequency.

Finally, the contributions of the individual sources may be added together, $P_{mB} = P_{Vm} + P_{Dm} + P_{Lm}$, to obtain the Fourier transform coefficient of the pressure at the m th harmonic of the BPF, whereas the far-field time domain pressure can be calculated directly from the Fourier transform.

2. *Asymptotic Analysis*

The Bessel function J_{mB} in Eq. (7) appears within the blade integral and affects both loading and thickness sources. Its argument $mBzM_t \sin\theta/(1 - M_x \cos\theta)$ equals $mBzM_t$ when $\theta = 90°$, the maximum value within the plane off rotation. The argument $mBzM_t$ remains essentially equal (or slightly smaller) to the order mB of the Bessel functions when its value peaks for subsonic tip Mach numbers suitable to regional and general aviation (GA) aircraft. The small argument asymptotic formula can be used to approximate this behavior. The asymptotic approximation of the Bessel function in Eq. (7) can be given by

$$J_{mB}\left(\frac{mBzM_t \sin\theta}{(1 - M_x \cos\theta)}\right) \sim \frac{1}{(mB)!} \left(\frac{mBzM_t \sin\theta}{2(1 - M_x \cos\theta)}\right)^{mB} \tag{11}$$

The near-field source distribution is defined through the sources terms Ψ_V, Ψ_L, and Ψ_D. The source terms contribute to defining the final spectrum shape and spectrum level, as the relative location between sources in the chordwise direction lead to destructive or constructive interference of the signals. The lift source strength Ψ_L depends on the chordwise distribution of lift or lift coefficient $C_L(x)$, which is assumed to be uniform. Respectively, Ψ_D is defined by a uniform drag distribution. The volume source Ψ_V represents the air displaced by the blade and is defined through the thickness-to-chord ratio t_b. A parabolic thickness distribution $H(x) = 1 - (2x)^2$ is assumed [25]. The source term transformations may then be estimated by combining the noncompactness effect relation with the proportionality realtion

$$\Psi_V(k_x) \approx \frac{1}{k_x^2} = \left(\frac{M_r(1 - M_x \cos\theta)}{2mBB_D M_t}\right)^2 \tag{12}$$

$$\Psi_D(k_x) = \Psi_L(k_x) \approx \frac{2}{k_x} = \frac{M_r(1 - M_x \cos\theta)}{2mBB_D M_t} \tag{13}$$

As a result, the source terms may be written as direct functions of the blade parameters, t_b, C_L, and C_D:

$$k_x^2 t_b \Psi_V(k_x) \approx t_b \tag{14}$$

$$k_x (C_D/2) \Psi_D(k_x) \approx C_D \tag{15}$$

$$k_y (C_L/2) \Psi_L(k_x) \approx \frac{C_L k_y}{k_x} \approx \frac{(M_x - M_r^2 \cos\theta)}{zM_t} C_L \tag{16}$$

To account for the entire blade, we assume that the thickness ratio at the blade tip takes the average value over the blade, $t_b(z = 1) = \bar{t}_b$,

and the loading coefficient, $C_D(z=1)=\bar{C}_D$ and $C_L(z=1)=\bar{C}_L$ (note that the loading parameters C_D and C_L may instead be defined in terms of thrust and torque, dT/dz and dQ/dz).

Combining the above and adding the contributions of the individual sources together, we may estimate $P_{mB}=P_{Vm}+P_{Dm}+P_{Lm}$ as

$$P_{mB}\approx\left(\frac{\rho_0 c_0^2}{8\pi}\right)\left(\frac{BD}{y}\right)\left(\frac{\sin\theta}{(1-M_x\cos\theta)}\right)M_h^2\left(\frac{1}{(mB)!}\right)\times\left(\frac{mBM_t\sin\theta}{2(1-M_x\cos\theta)}\right)^{mB}\left[\bar{t}_b+\frac{\bar{C}_D}{2}+\frac{\bar{C}_L(M_x-M_h^2\cos\theta)}{2M_t}\right]\times\exp\left[imB\left(\frac{\Omega r}{c_0}-\frac{\pi}{2}\right)\right] \tag{17}$$

Sound intensity and therefore overall acoustic power is proportional to p_{rms}^2, and we have

$$p_{m,\text{rms}}^2=\langle P_{mB}P_{mB}^*\rangle\approx\underbrace{\left(\frac{\rho_0 c_0^2}{8\pi}\right)^2}_{\text{constants}}\underbrace{\left(\frac{1}{y}\right)^2}_{\text{Spherical Spreading}}\times\underbrace{B^2D^2M_h^4\left[\bar{t}_b+\frac{\bar{C}_D}{2}+\frac{\bar{C}_L(M_x-M_h^2\cos\theta)}{2M_t}\right]^2}_{\text{Design/operation parameters}}\times\underbrace{\left(\frac{\sin\theta}{(1-M_x\cos\theta)}\right)^{4mB+2}}_{\text{Directivity}}\underbrace{\left(\frac{1}{(mB)!}\right)^2\left(\frac{mBM_t}{2}\right)^{2mB}}_{\text{Spectral Shape}} \tag{18}$$

Equation (18) represents the main expression to be used for the development of the scaling laws. Helpful deductions may be made by the interpretation of the asymptotic approximation. For subsonic tip Mach numbers $M_t<1$, the exponential term M_t^{2mB} indicates that the acoustic energy in each mode decreases with harmonic order m. The same relation is true for blade number.

The presence of $\sin\theta$ in the Bessel function argument of Eq. (7), and hence in the approximation relation Eq. (18), results in the propeller's well-documented dipole behavior. As the propeller axis is approached from both front and back, the radiated noise decreases. Furthermore, the Doppler factor $(1-M_x\cos\theta)$ causes the directivity pattern to move into the forward arc with regard to the propeller plane.

By setting $m=1$ in to Eq. (18), the absolute level of the fundamental tone for the baseline case $p_{f_{1_0}}$ and the modified case p_{f_1} may be estimated. Subsiquently, by substituting into Eq. (5), the change in fundamental tone noise level is given by,

$$\begin{aligned}\Delta L_{f_1}=&\,20\log_{10}\left(\frac{y}{y_0}\right)+20\log_{10}\left(\frac{BD}{B_0D_0}\right)+40\log_{10}\left(\frac{M_h}{M_{h_0}}\right)\\&+20\log_{10}\left(\frac{t_b+\bar{C}_D+\bar{C}_L(M_x-M_h^2\cos\theta)/(M_t)}{t_{b,0}+\bar{C}_{D,0}+\bar{C}_{L,0}(M_{x,0}-M_{h,0}^2\cos\theta_0)/(M_{t,0})}\right)\\&+20\log_{10}\left(\frac{B_0!}{B!}\right)+20\log_{10}\left(\frac{(BM_t)^B}{B_0M_{t,0})^{B_0}}\right)\\&+20\log_{10}\left(\frac{[\sin\theta/(1-M_x\cos\theta)]^{2B+1}}{[\sin\theta_0/(1-M_{x,0}\cos\theta_0)]^{2B_0+1}}\right)\end{aligned} \tag{19}$$

where the subscript 0 denotes the values corresponding to the condition before the modifications were applied (baseline).

Separating all terms including the mode number m in Eq. (18), we may define a function S. This function determines the shape of the harmonics.

$$S(m)=\left(\frac{\sin\theta}{1-M_x\cos\theta}\right)^{4mB+2}\left(\frac{1}{(mB)!}\right)^2\left(\frac{mBM_t}{2}\right)^{2mB} \tag{20}$$

Normalizing this expression by its value for $m=1$,

$$\bar{S}\left(\frac{f}{f_1}\right)=\frac{S(m)}{S(1)}=\left(\frac{\sin\theta}{1-M_x\cos\theta}\right)^{4B(m-1)}\times\left(\frac{B!}{(mB)!}\right)^2\left(\frac{BM_t}{2}\right)^{2B(m-1)}m^{2mB} \tag{21}$$

noting that $\bar{S}(1)=1$ by definition. Finally the change in level of the harmonics ($m>1$) between a baseline case and a modified counterpart may be given by

$$\begin{aligned}\Delta F_1\left(\frac{f}{f_1}\right)=&\,20m\log_{10}\left(\frac{m^B}{m^{B_0}}\right)+20\log_{10}\left(\frac{B!(mB_0)!}{B_0!(mB)!}\right)\\&+20\log_{10}\left(\frac{(BM_t)^{B(m-1)}}{(B_0M_{t,0})^{B_0(m-1)}}\right)\\&+40\log_{10}\left(\frac{[\sin\theta/(1-M_x\cos\theta)]^{B(m-1)}}{[\sin\theta_0/(1-M_{x,0}\cos\theta_0)]^{B_0(m-1)}}\right)\end{aligned} \tag{22}$$

D. Propagation and Corrections

Once the source levels of the novel aircraft have been estimated, the NPD flyover procedures may be implemented, which include propagating the source levels to the observer locations on the ground. The standard recommendation of Doc29 is used for propagation and atmospheric attenuation/absorption, namely, SAE ARP 866A [5] for atmospheric absorption modeling and SAE AIR-1845 [3] for the procedure of generating the complete NPD data sets. Finally, standard A-weighting (IEC 61672 or ANSI S1.4) is applied at the observer location in the cases where the metrics required it. Note that the same algorithms are used when backpropagating NPD data to the source, just applied in reverse. Standard atmospheric conditions are assumed at all times, i.e., $p_0=101.325$ kPa and $T_0=15.0$°C. For exposure metrics, the standard duration adjustment is applied when required, assuming the aircraft reference speed V_{ref} to which the baseline NPD data relate.

E. Assumptions

A summary of the modeling assumptions is presented below, first for the lumped source model for whole air vehicles noise and then for the specific propeller harmonic noise source method as implemented.

List of assumptions for lumped source model:

1) The individual noise sources that make up the lumped source are assumed to be incoherently added to provide a total PWL representative of the whole vehicle's acoustic radiation.

2) Individual noise sources are all assumed to be located at one location onboard the air vehicle, typically the center of gravity; this defines the lumped source as a single point source representation of the air vehicle.

3) All individual noise source emission reference frames are aligned and combined to give the total air vehicle's emission angles, as in Fig. 3.

4) The directivity and spectral content of the final lumped source are defined by a sound power-weighted sum of those of the individual noise sources; directivity is assumed not to be frequency dependent.

5) The PWL of the novel/concept cases is calculated using a linear interpolation from a baseline case, as demonstrated earlier in the section and validated in the following section.

A list of assumptions for the propeller tonal noise method derived herein:

1) Beyond the "thin-blade" assumption of the original Hanson model, the propeller geometry and loading characteristics are assumed to be constant in the radial direction, using representative average values. This assumption manifests in the compactness of the source region on the blade.

2) The radiation efficiency is determined by the small argument asymptotic approximation of the Bessel function.

3) The simplified method is used to calculate changes to the PWL of propeller steady harmonic noise and changes in the tonal distribution of the frequency spectrum; these are then implemented within the lumped source model.

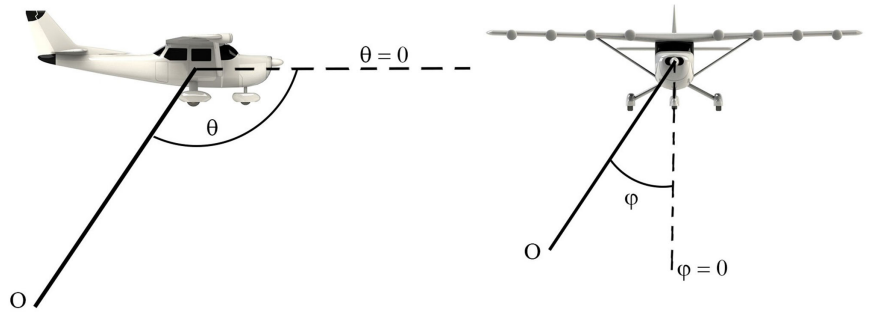

Fig. 3 Polar and azimuthal emission angles. Adapted from [20].

IV. Error Analysis

In Sec. III, the methodology for calculating the propeller discrete noise fundamental tone of some novel scenario was presented. The calculation requires knowledge of the baseline level and some Δ correction as

$$L_{f_1} = L_{f_1,0} + \Delta L_{f_1} \tag{23}$$

ΔL_{f_1} is by definition the difference of the level in dB produced by the baseline and the modified scenario of interest. In some cases, this may be called the absolute difference. However, in order to practically evaluate ΔL_{f_1} using the Hanson model as in Sec. III.C, a linear approximation assumption is used. Virtually, this means that the estimated change in noise neglects the changes in the higher-order terms. The crux of this assumption is that the linear approximation is performed on the logarithmic output function of the noise. The linear approximation is explained in detail in Appendix A.

This section compares the linear approximation with the exact variation in the noise function on a dB basis. The calculations are performed for a single propeller whose design and operation parameters are varied. The error ϵ is defined as a relative error:

$$\epsilon = \left\| \frac{f - g}{f} \right\| \tag{24}$$

where f represents the exact value of the functions, while g the linear approximation. Figure 4 shows the error between the actual function values and the linear approximation for four different parameters. The chosen baseline point has parameters of diameter $D = 1.4$ m,

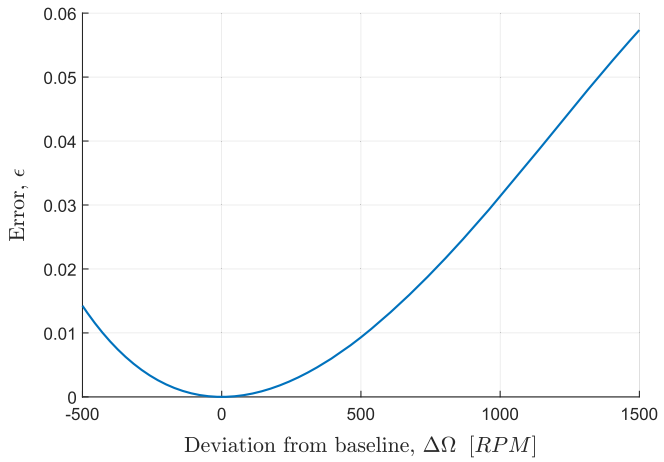

a) Relative error ϵ as a function of change in propeller rpm

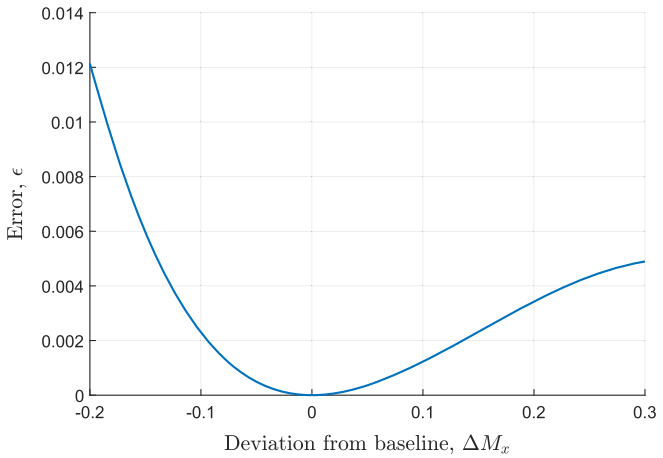

b) Relative error ϵ as a function of change in flight mach number

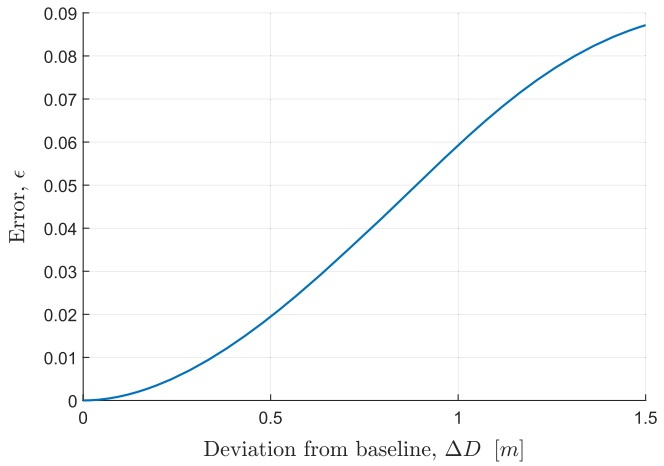

c) Relative error ϵ as a function of change in propeller diameter

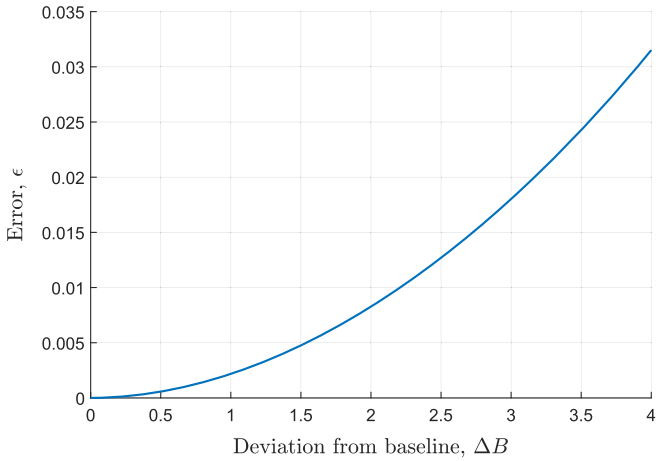

d) Relative error ϵ as a function of change in number of propeller blades

Fig. 4 Approximation error as a function of change in parameters $\Delta\eta_j$.

number of blades, $B = 4$, flight Mach number $M_x = 0.4$, and rotational speed of $N = 2000$ rpm. The x-axes portray $\Delta\eta_j$ as the prediction start to deviate from the baseline, where j indexes through parameters η. The error remains small ($\epsilon < 0.1$) even for relatively large changes.

V. Validation: Predictions for Regional Aircraft

A validation of the proposed framework is presented next using noise and performance data of existing propeller powered aircraft. The source of the data is the ANP database, where performance characteristics of the aircraft are provided for the aircraft takeoff and landing operation as well as noise data, in the form of NPD curves in instantaneous and cumulative metrics such as $L_{A,\max}$, SEL, and effective perceived noise level (EPNL). Additional design and operation characteristics are obtained from certification documents such as the European Aviation Safety Agency (EASA) type certificate data sheet (TCDS) and type certificate data sheet (for noise) (TCDSN) [26,27].

The validation process is as follows: For each aircraft the takeoff operation is considered. A singular point on the published ANP departure $L_{A,\max}$ NPD curves is appointed as the baseline point. This point corresponds to a particular takeoff configuration of power setting j generating level $L_{A,\max}$ during a flyover of slant distance d.

The presented framework is then employed to estimate changes ΔPWL relative to this baseline point for the rest of the NPD power settings $j_1, \ldots, j_n$, where n is the total number of power settings. The predicted levels are then propagated to the rest of the slant distances to complete the NPD data set for that aircraft performing a departure operation. The predicted NPD set is then compared to the rest of the published ANP data set. In Appendix B, the process for computationally creating the NPD curves is discussed in detail.

Predictions for two fixed-wing propeller power aircraft are presented in Figs. 5 and 6. Specifically, the aircraft chosen are the DHC-6 Twin Otter and the larger turboprop ATR 72-212A. A summary of the design and performance characteristics may be seen in Table 1. Two additional cases are presented in the supplementary material for this paper, the Cessna 172 and the Britten Norman BN-2 Islander.

For all cases, the baseline point was at a slant distance of 304.8 m, and it is depicted by a black cross. The published data are represented by dashed lines, whereas the predicted data are represented by solid lines.

The first validation case shows the feasibility of predicting NPD curves for traditional turboprop aircraft, specifically, the DHC-6

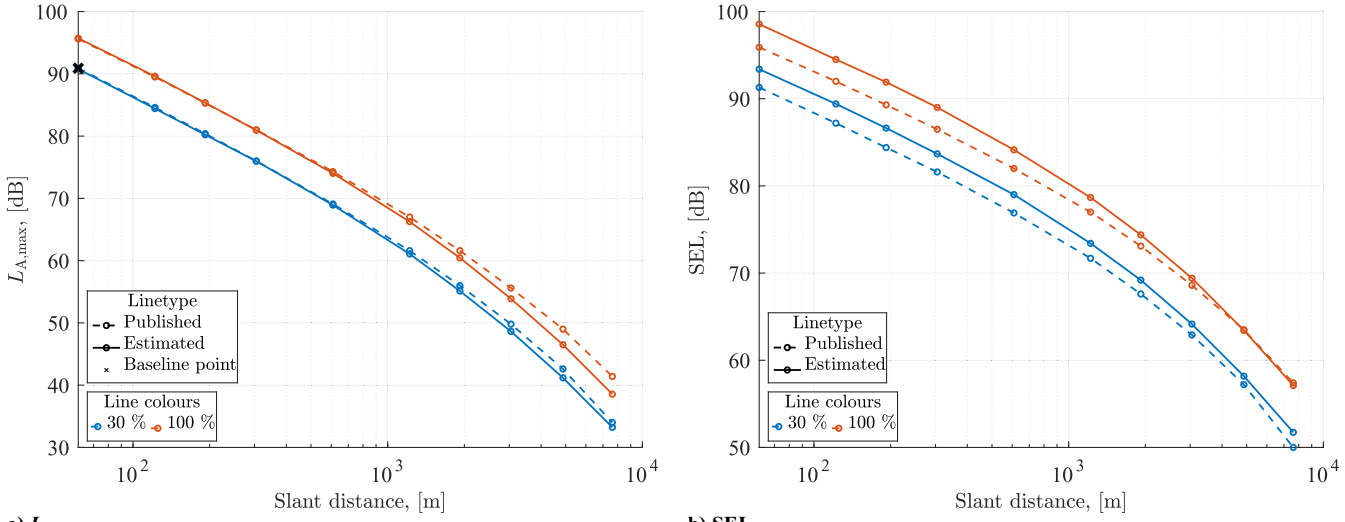

a) $L_{A,\max}$ **b) SEL**

Fig. 5 Takeoff NPD curves for a twin-engine de Havilland Canada DHC-6 (Twin Otter). Solid lines indicate the predicted levels, whereas dashed lines are the baseline aircraft published NPD data.

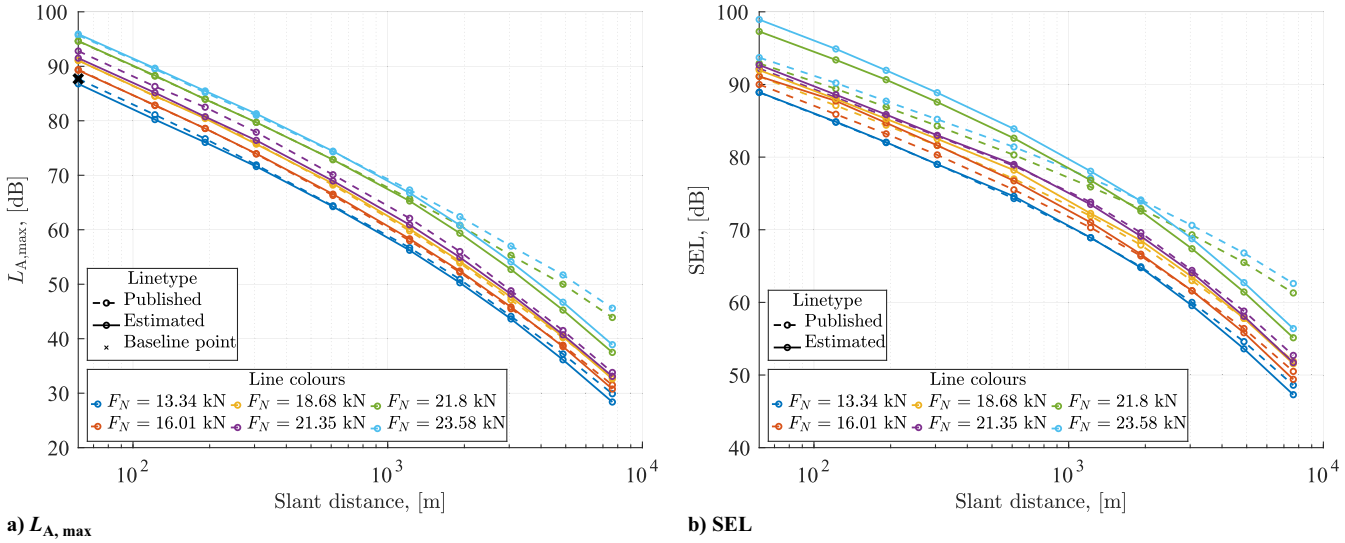

a) $L_{A,\max}$ **b) SEL**

Fig. 6 Takeoff NPD curves for a twin-engine turboprop ATR 72-212A. Solid lines indicate the predicted levels, whereas dashed lines are the baseline aircraft published NPD data.

Table 1 Validation aircraft performance and design parameters

Aircraft	MTOW, kg	Prop diameter, m	No. of blades	Takeoff, rpm
DHC-6 Twin Otter	5,670	2.6	3	2,110
ATR 72-212A	22,800	3.93	6	1,200

Twin Otter (maximum takeoff weight [MTOW] 5682 kg, still within the ICAO Annex 16 [28] defined as "small," referring to Chaps. 6 and 10) with a twin-engine configuration. The estimated NPD curves may be seen in Fig. 5 relative to the measured ANP NPD curves for the Twin otter. The power settings shown are 30 and 100% of maximum static thrust (MST).

Figure 6 compares the estimated versus published NPD curves sets for the significantly larger ATR 72-212A. Power settings were chosen according to the stated values of corrected net thrust (CNT) at the measurement points. The power setting parameter values, in both cases, are given on a per engine basis.

To understand the results, the NPD curves are split into two components: i) the estimation of the first point on any given power curve, and ii) the extrapolation to all other slant distances at a given power setting j.

The first component is a direct result of estimating the change in overall PWL of the aircraft in question using the framework described in this paper. The first point on the baseline power curve (i.e., the chosen baseline point), as expected, matches almost perfectly with the measured data. This is explained as all delta terms added to the baseline levels are zero, retrieving the baseline levels themselves. The only slight discrepancy is caused by the point of occurrence of the $L_{A,\max}$ during the NPD flyover event. The strong dipole-like directivity assumption, influenced by the propeller method, causes a mismatch relative to the published data, contributing a small delta.

Next is the estimation of all other power settings at the same slant distance as the baseline point. The same small $L_{A,\max}$ related delta is carried through all power settings, although not constant, as the directivity is a function of the power setting. The ΔPWL between power settings is estimated predominantly (airframe noise deltas are also accounted for with minor contributions in the high-power departure operations) using the asymptotic relations for the propeller method derived in this paper. Looking at the $L_{A,\max}$ plots in Figs. 5 and 6 at the baseline slant distance of 60.96 m (200 ft), the method captures the changes in the overall PWL and spectral content distribution and the resulting propagation of the flyover event adequately, with an average error of ± 0.4 dBA ($L_{A,\max}$). It is observed, however, that the error increases significantly as points further away from the baseline point are predicted. This is expected, given the error analysis in Sec. IV. This could be mitigated by using different baseline points for each power curve prediction (although this is avoided as, in many cases, baseline NPD curves are limited, requiring a larger deviation from the baseline point).

As explained in Appendix B, all points on an SEL power curve are estimated computationally; this means that the same $L_{A,\max}$ level is used as a baseline. As established, the estimation of the overall PWL is reasonable for the point of $L_{A,\max}$, and, therefore, as power is constant over the flyover event, we may assume that this is the case for the entire event. This leads to deviations in the SEL results for the baseline 60.96 m slant distance as a result of two factors, the polar directivity over the exposure metric integration interval of $0 < \theta < 180°$ and spectral content. The purely dipole nature of the assumed polar directivity results in noise levels diminishing for angles of θ approaching 0 and 180 deg. For small slant distances, this effect has little impact, as the levels diminish outside the 10 dB down window in the estimation of the SEL.

The impact of spectral content on the SEL is threefold. First, the assumption that directivity is constant with frequency impacts the overall aircraft's directivity with the knock-on effects previously discussed. Second, because atmospheric attenuation is frequency dependent, it could contribute to underprediction in the case of a lumped source model dominated by midfrequencies to high frequencies and overprediction in the opposite case. In the case of the presented framework, the only adjustment to the spectral content is the level and shifting of the propeller BPF harmonics. However, both presented cases use constant-speed propeller setups, resulting in the frequency content (not level) between power settings being the same. Attenuation-related errors are therefore the result of not appropriately adjusting the spectral content. This suggests that the lumped source definition is incomplete, especially for low slant distances. Inclusion of a propeller broadband noise method would contribute the overall PWL at low slant distances and also "fill in" the directivity in the propeller axial directions, correcting the prediction of higher slant distances. The third and final impact of the spectral content on an SEL calculation is the A-weighting. As known, the A-weighting adjusts the OASPL to account for the higher sensitivity of the human ear in the 1000–10,000 Hz range, meaning that the low-frequency tonal content of propeller noise contributes less to an A-weighted noise level L_A, suggesting another source of possible underprediction.

The second part of the calculation is the extrapolation to all other slant distances beyond the baseline slant distance. This process follows exactly that of the SAE-AIR1845A [3]. This is based on the knowledge of the measured $L_{A,\max}$ at a particular slant distance as the starting point. In our case, this is the lumped-source-model-predicted $L_{A,\max}$. In addition to the dynamics discussed between the directivity, spectral content, and propagation distances that affect the final extrapolation, an additional assumption is used within SAE-AIR1845A. This is known as the "simplified adjustment procedure," an additional source of possible error discussed later in the text.

To summarize, variations and discrepancies between the predictions and published data may be explained by considering two main factors:

1) Deviation of the assumed idealized dipole nature of propeller harmonic noise directivity with the actual aircraft directivity at the time of the measurements: The effects of the dependence of noise on the ground directly beneath the flight path on distance (spherical spreading) and directivity changes from one flyover altitude to another.

2) Limited baseline spectral data: The ANP database provides a single one-third octave band spectral breakdown for aircraft of specific categories [2,29]. Therefore the reference spectral content may not be aircraft or power setting specific, allowing for greater "distance" between the baseline point and the intended calculation.

Despite the sources of error described, the arithmetic average of the difference between the published and predicted NPD curves across all aircraft, power settings, and slant distances was ± 1.5 dB for the $L_{A,\max}$ NPD curves and ± 2 dB for the SEL NPD curves, both of which are within the ECAC Doc 29 [2] tolerance. Additional insight into possible sources of error is discussed in Sec. VII.

The cases presented vary in the design decisions when it comes to propeller blade design and operating envelopes; however, changes in both of these categories may be captured and quantified on a high-level basis as presented.

VI. Application: Concept Aircraft NPD Predictions

To demonstrate the capabilities of the proposed framework, NPD curves are calculated for three hydrogen-powered regional concepts, provided by project NAPKIN [30]. These concepts are based on current flying aircraft, namely, the DHC-6 Twin Otter and the ATR72-600. The concepts will be referred to as Concept B5, Concept B8, and Concept E1. Concepts B5 and B8 are based on the Twin Otter, while Concept E1 on the ATR72-600. Details of the designs as well as important performance parameters relevant to the NPD calculations may be found in Appendix C.

To accurately represent the concept aircraft in terms of the acoustic lumped source model, in addition to the framework assumptions (Sec. III.E), a series of case-study-specific assumptions are made:

1) The aircraft as a noise source comprises the contributions of two individual sources: the propeller tonal noise and the airframe components. This assumption is reasonable as demonstrated in the validation in Sec. V and further discussed in Sec. VII.

2) The estimation of the baseline level of the individual sources is based on a methodology developed by Synodinos et al. [1,20]. The breakdown of the total aircraft noise source into individual components is based on data within [22,31].

3) As a result of the dominant sources being propeller self-noise and airframe noise, the directivity factor of the lumped source is given by the combination of the directivity of the propeller (seen in Fig. 7) and the "dipole-like" directivity of the airframe noise component given in Ref. [32]. The directivity factor of the individual sources is combined as a weighted sum, with the weight being the individual PWL level of the respective sources. This is shown in [1].

4) The high-level performance data required for the reference aircraft are acquired from open-source databases such as the ANP database [21], EASA TCDS, and TDCSN certificates [26,27] as well as factsheets by manufacturers [33].

5) The spectral content of the reference aircraft is limited to the data provided by the ANP database. For each aircraft, 1/3rd octave band frequency breakdown is provided for takeoff and approach configurations. The levels are unweighted given at a slant distance of 305 m for center frequencies ranging from 50 Hz to 10 kHz.

Prediction risks: It is important to identify potential additional sources of noise that are unique to the hydrogen concepts discussed herein and that could have the potential of dominating the sound profile under specific operating conditions and/or emission angles if care is not taken. In addition to the risks of additional sources, the noise prediction methodology used does not account for noise abatement design choices implemented or planned for the concept aircraft. Examples of such design choices could be the use of fan intake liners or the use of novel propeller/fan designs for quiet operation.

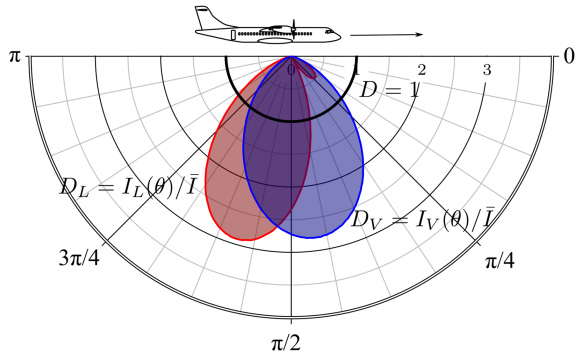

Fig. 7 Polar plot of propeller loading D_L and thickness (volume) D_V noise directivity factors as derived by Hanson [23]. Polar angle θ is measured from the flight axis in the direction of flight.

1) Multiple propeller interactions: There are interactions between individual propeller potential fields, and there are wake/tip–vortex interactions with or without the interference of the propeller structure itself.

2) Propeller–airframe interaction: Interaction of airframe component potential fields with the propeller field causes unsteady effects on noise-generating mechanisms, and propeller wakes interact with the airframe structure and vice versa.

3) Fuselage scoop/intake noise: Flow over open cavities or cutouts in the surfaces of aircraft often produces intense pressure oscillations in the cavity, which radiate discrete noise. Such design features could be a result of cooling systems being implemented.

4) Hydrogen combustion noise: Flame attachment due to the high reactivity of H_2 has a significant effect on how low-swirl injectors respond to self-excited flame oscillations. This leads to significantly higher acoustic driving due to the compact shape of the flame and its flame folding dynamics. Mitigation of flame attachment and/or deferring the formation of the outer shear layer is needed to avoid such dynamic noise generation mechanisms. Approach operations are at risk due to the higher impact of core noise and possible higher idling power settings to maintain flame.

5) Electric motor: The dominant source of noise in electric motors comes from the interaction of a rotor and stator that induces vibration of the motor frame. Preliminary research shows that levels are expected to be low compared to other propulsion noise sources like the fan; however, it is possible that a portion of a flyover during approach will include motor noise depending on the motor installation.

A. Departure

For the departure NPD curves, a single power setting is calculated for the concept aircraft. The power setting is assumed to be at MTOW. The thrust requirements for takeoff at MTOW may be found in Table C1 of Appendix C. Figures 8–10 show the $L_{A,\max}$ and SEL NPD curves for the three concept aircraft.

As all concepts are in the conceptual (or early preliminary) design stage, operational thrust profiles have not yet been fully defined. The comparisons in Figs. 8–10 are therefore between a single full-power takeoff at MTOW between the reference aircraft and the concepts. The concepts are designed to match the flying performance of the respective reference aircraft (this is a starting assumption and is explored in detail as a part of the contribution of the entire NAPKIN consortium; e.g., aircraft performance may not dominantly drive aircraft take-up by airlines as costs and infrastructure development may cause tradeoff scenarios). This also ensures that, for the concepts, the maximum number of passengers are carried.

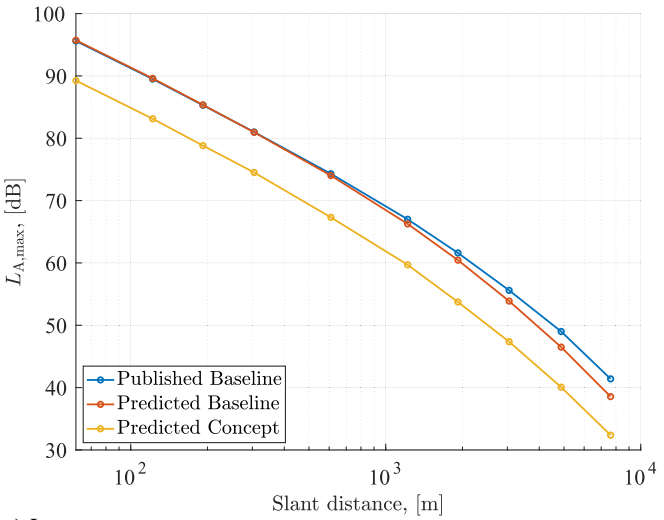

a) $L_{A,\max}$

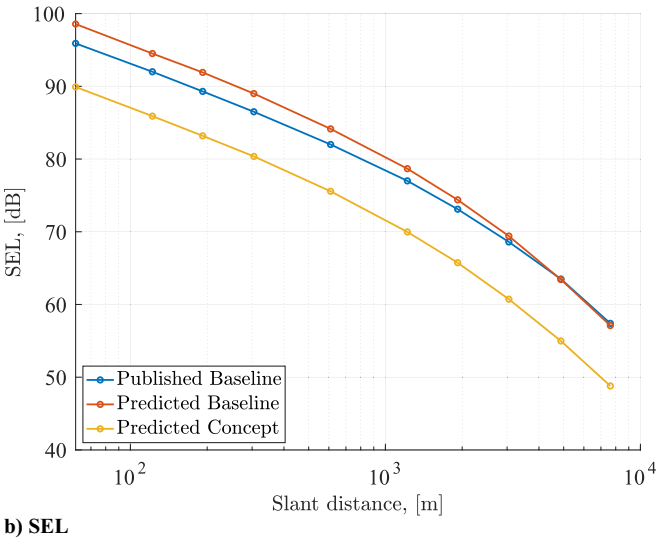

b) SEL

Fig. 8 Estimated departure NPD curves for Concept B5, compared against the published ones of the reference aircraft DHC-6 Twin Otter.

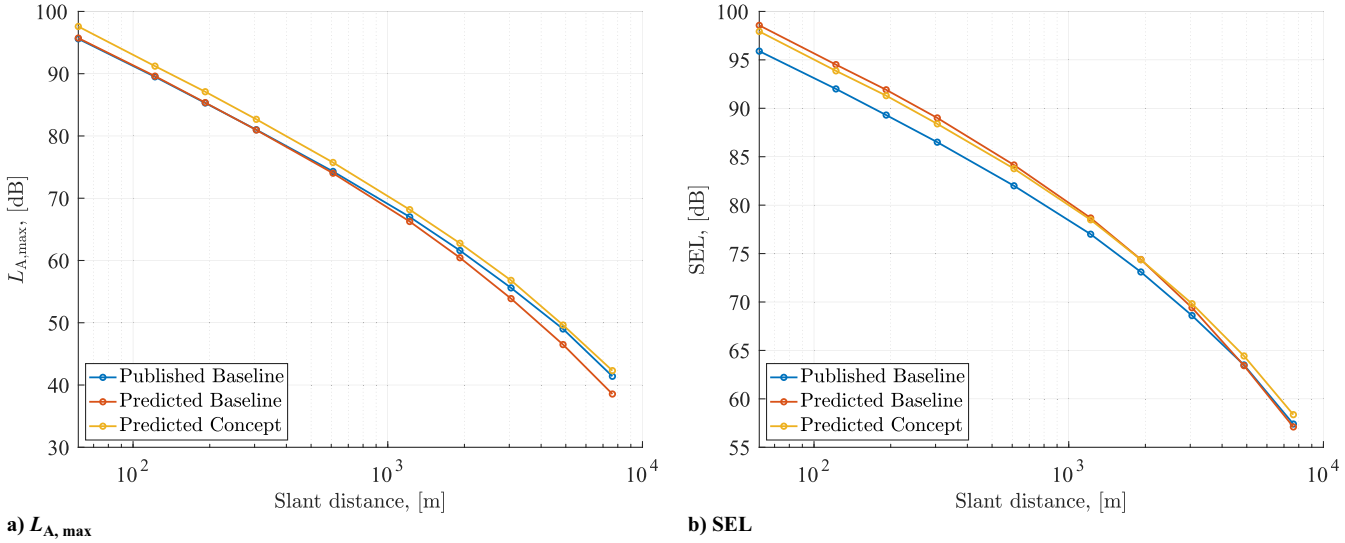

a) $L_{A,\,max}$ **b) SEL**

Fig. 9 Estimated departure NPD curves for Concept B8, compared against the published ones of the reference aircraft DHC-6 Twin Otter.

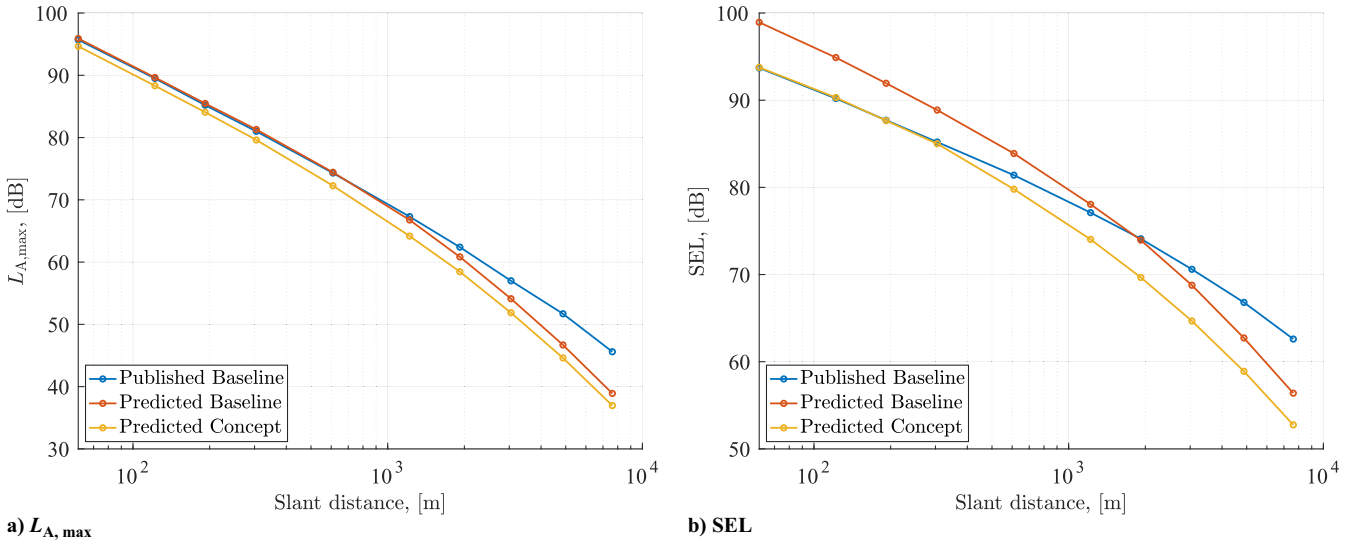

a) $L_{A,\,max}$ **b) SEL**

Fig. 10 Estimated departure NPD curves for Concept E1, compared against the published ones of the reference aircraft ATR72-212A.

The NPD curves in Figs. 8–10 compare the published NPD data for the baseline aircraft with the predicted NPD data for the baseline and finally the NPD data for each of the concepts. Importantly, all curves represent a full-power maneuver at MTOW for each aircraft. Arguably, a comparison normalized to MTOW (or net thrust) would provide a clearer picture of the impact design decisions have on noise output. However, the 1-1 comparison of current technology aircraft and concepts using hydrogen propulsion systems provides insights within the context of understanding the noise impact of aircraft fleets transitioning to zero emissions. A study conducting a sweep of operational MTOW would be the next step in the process, when designs are consolidated and more mature.

Investigating the maximum engine power setting NPD curve allows for the possibility of calculation of noise at the certification points and comparison to the appropriate limits of the ICAO Annex 16 [28].

Concept B5 shows the greatest noise benefits relative to reference aircraft, irrespective of the increased MTOW. Characteristics that contribute to the reduction in noise are i) reduction in the loading of individual propellers due to the increase in the number of propellers from 2 in the reference Twin Otter to 4 in the case of the concept (although the major contribution to loading noise is predominantly the lift component, a reduction in the drag noise source is also observed due to a reduction in the power requirement per propeller), and ii) reduction of rotational speed at takeoff and landing conditions. A reduction in tip Mach number from 0.8472 to 0.8072 has a significant effect, as operation is already in the transonic regime.

As with Concept B5, the reference aircraft for Concept B8 is again the DHC-6 Twin Otter. Despite the huge difference in MTOW (10,000 kg for the Concept B8 and 5670 kg for the Twin Otter), the thrust requirement has only increased by approximately 21%. It is important to note that the Twin Otter is certified under Chapter 10 of the ICAO Annex 16 [28]; however, Concept B8 exceeds the MTOW limit and would be certified under Chapter 14. The tip Mach number $M_t = 0.7454$, which is reduced relative to the reference aircraft, and the increase in the number of blades from 3 on the Twin Otter to 5 account for additional noise reduction.

The NPD curve behavior for Concept E1 is predominantly driven by changes in MTOW relative to the ATR72-600. Lower thrust requirements intrinsically reduce the loading components of propeller harmonic noise (both lift and drag). As the operation and design of the turboprop blades were assumed to be identical to those of the reference aircraft, the thickness noise and propeller tip Mach number effects are therefore the same as those of the reference aircraft. Additional benefits to propeller noise may be achieved by altering the propeller geometry and operational revolutions per minute (rpm) to take advantage of the lower disk loading.

B. Approach

The approach operation and certification point require additional considerations. Limited data are available for all concepts for the approach operation. As maximum landing weight (MLW) thrust requirements and high-lift devices have not been provided, it was decided to model the approach performance using the percentage of maximum takeoff thrust. Using performance data of the reference aircraft at MLW approach conditions, ratios of MLW to MTOW thrust were calculated. In addition to MLW performance settings, the same ratios were calculated for the minimum landing power setting (minimum landing weight) available in the ANP database for the reference aircraft. These ratios were then used on the concept MTOW to estimate the approximate maximum and minimum lading power settings. The resulting ratios are presented using the percentage in Table 2.

Although these values may not be the realistic operational values of thrust, this method allows for direct comparison to the reference aircraft while also providing a possible range within which the aircraft might be expected to lie. Assuming identical percentage of maximum takeoff thrust assumes that the concepts have the same landing performance (lift and drag characteristics, etc.) as the reference aircraft. This might be the case for retro-fit designs, while clean sheet designs might look to improve on the reference design. Alterations to the drag profile of an aircraft at approach are likely to be accompanied by an alteration in engine power settings, and therefore additional power settings may be needed to complete an NPD curve set for approach. Where given, landing airspeeds have been taken into account.

The baseline noise levels were derived from NPD data for the reference aircraft and approach NPD curves for the power settings mentioned above. Specific 1/3rd octave band spectra from the ANP database for the approach are also used for the baseline aircraft.

Approach NPD curves were estimated using a percentage of the maximum takeoff thrust used by the reference aircraft. The NPD curves may be seen in Figs. 11–13. As previously mentioned, the dashed lines represent the published NPD curves for the baseline aircraft, the dotted lines represent the estimated NPD for the baseline aircraft (only in the $L_{A,\max}$ figures), and the continuous lines are the estimated approach NPD curves for the concept aircraft. The indicated "min" and "max" power settings are the ones equivalent to Table 2. The stated baseline point (level) is indicated with a black cross on the $L_{A,\max}$ figures at a slant distance of 60.96 m (200 ft).

Table 2 Approach power settings based on percentage of MTOW takeoff thrust

	Minimum power setting		Maximum power setting	
Concept	Percentage	Thrust, kN	Percentage	Thrust, kN
B5	30.00	0.96	100.00	3.20
B8	30.00	2.91	100.00	9.70
E1	16.70	3.26	30.00	5.85

Maximum and minimum power settings replicate those of the approach NPD curves in the ANP database for each reference aircraft.

The first observation is made against the prediction for the baseline. In all cases, a slight overprediction is observed in the $L_{A,\max}$ noise levels relative to the published data for both power settings. The main factors influencing this difference are, as discussed in the departure case, the whole aircraft's directivity and spectra. Additionally, this slight overprediction might indicate a bias toward the propulsion sources in the noise breakdown, suggesting a calibration of the breakdown for approach is necessary.

Concept B5 approach noise is expected. Despite the slight increase in MTOW, the additional two propellers allow for lower landing thrust to be achieved through reduced rpm and significantly different loading conditions. Additionally, the preferential flap deflection angle of 20 deg relative to the reference aircraft (37.5 deg) significantly reduces the airframe contribution. No additional changes to the airframe design relative to the Twin Otter are provided, suggesting no major sources of underprediction.

Approach noise levels for Concept B8 are the most interesting of the three concepts. As mentioned, the predictions for the baseline are slightly higher for both power settings relative to the published NPD curves. However, relative to that prediction, the "min" power setting suggests lower $L_{A,\max}$ levels for the concept at lower slant distances, while that difference diminishes for larger slant distances. This effect is predominately driven by the directivity differences due to the ducted-fan architecture of concept B8. At low slant distances, the blockage (redistribution of noise radiation into two distinct forward and rear arc lobes, as opposed to the dipole lobe [Fig. 7] of the reference aircraft). The observer is in the direction OF the peak of the ducted-fan directivity at a greater distance (further away from the closest point of approach). At higher slant distances, the maximum emission angle offset between the two cases is reduced, minimizing the effect of spherical spreading at the point of $L_{A,\max}$ and almost equalizing the maximum level observed.

For the "max" power setting, on the other hand, the concept is very slightly louder across all slant distances. A result was expected due to the significantly larger MTOW and landing airspeed. This result is perhaps on the optimistic side of the spectrum for Concept B8 at approach, as detailed airframe/landing gear design has not been accounted for in the airframe noise contribution.

The results for Concept E1 are unsurprising. The reduction in MTOW is reflected in the power setting percentages chosen, and therefore a reduction in noise is observed in the approach event. The

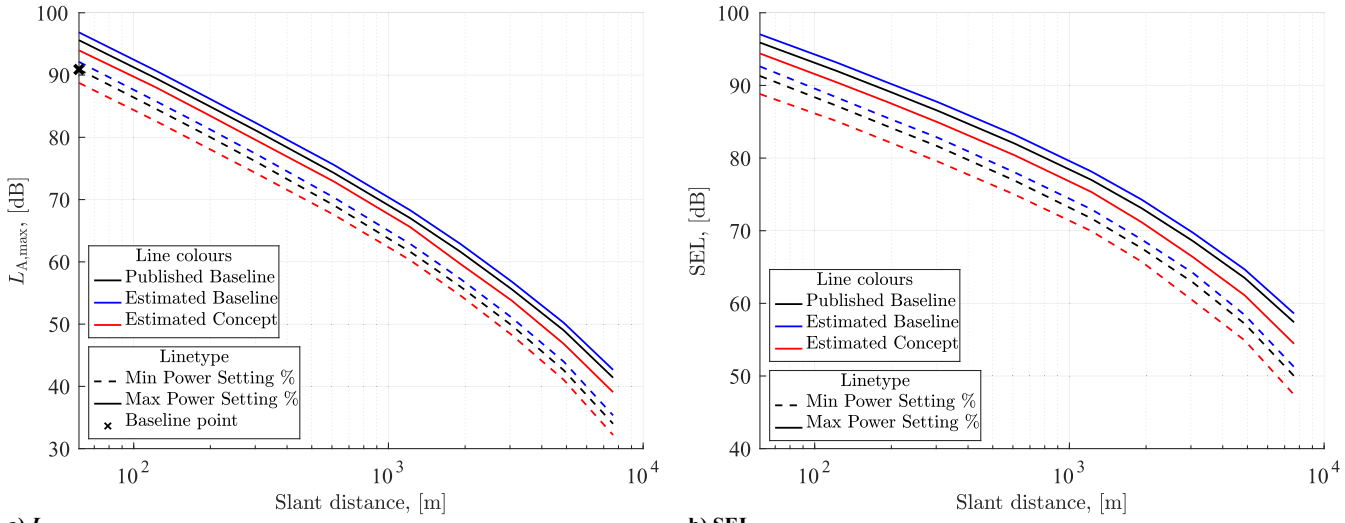

a) $L_{A,\max}$ **b) SEL**

Fig. 11 Estimated approach NPD curves for Concept B5, compared against the published ones of the reference aircraft DHC-6 Twin Otter.

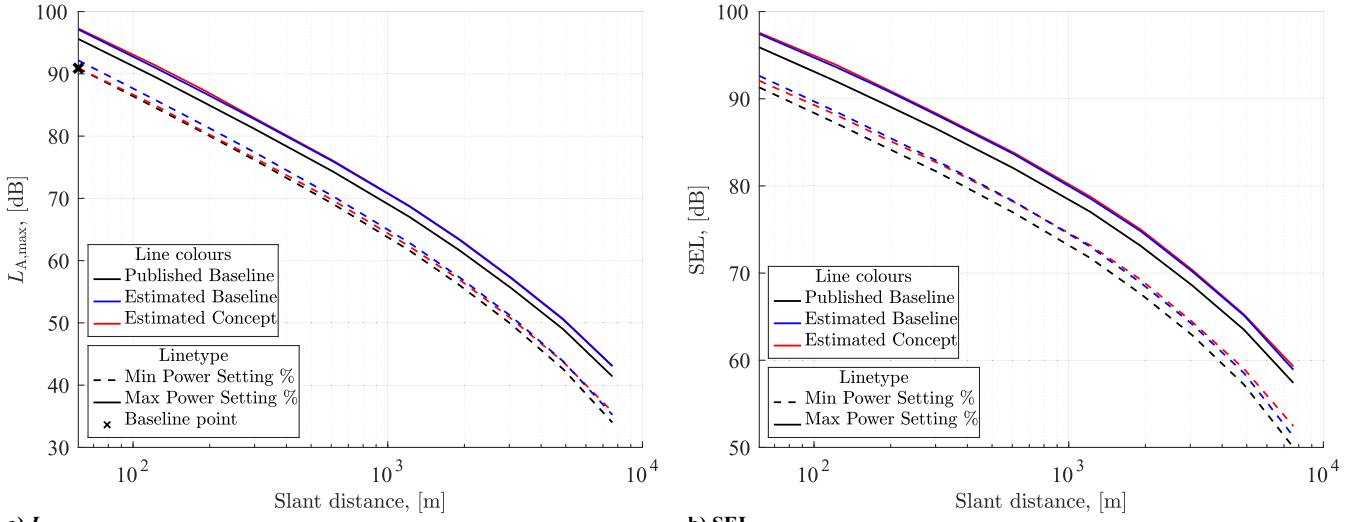

a) $L_{A,\,max}$ **b) SEL**

Fig. 12 Estimated approach NPD curves for Concept B8, compared against the published ones of the reference aircraft DHC-6 Twin Otter.

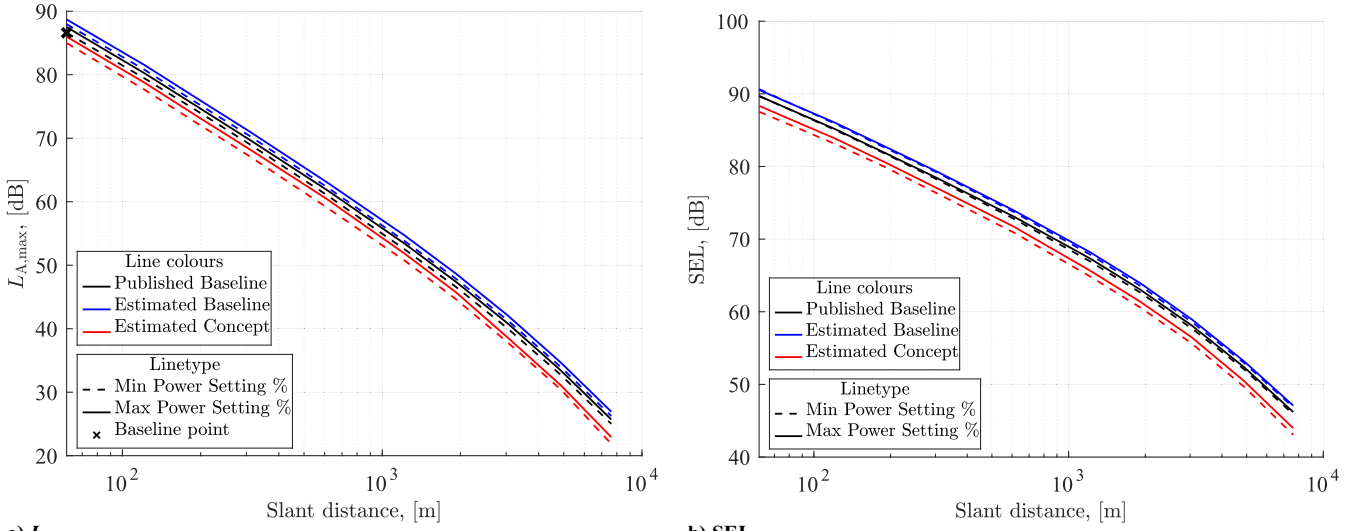

a) $L_{A,\,max}$ **b) SEL**

Fig. 13 Predicted approach NPD curves for Concept E1, compared against the published ones of the reference aircraft ATR72-212A.

airframe and landing gear design are unchanged relative to the ATR-72, resulting in the minor changes in levels being attributed to the change in landing speed from 61 to 58.1 m/s, contributing to the reductions. Further reductions would be observed in the comparison of the approach certification point due to the slightly steeper approach angle.

C. Summary

Concepts with an increased number of propellers, number of blades, and diameters and reduced rotational speed relative to the reference aircraft benefited in terms of maximum observed SPL and SEL at both takeoff and approach. Observed noise variations in takeoff noise levels are more apparent due to propeller noise being the dominant source.

Despite the increase in MTOW and thus thrust requirements, Concept B5 shows reductions in all aspects of the noise power distance curves. Significant decreases are observed at full-power takeoff as the engine (specifically propeller) sources dominate throughout the operation. This trend of reduced noise levels by increasing the number of propellers is further validated by the comparison of the already certified de Havilland Canada DHC-7 with the similarly sized DHC-8. The four turboprop configuration of the DHC-7 leads to significantly reduced noise certification levels at all three points relative to almost all variants (lighter and heavier) of the DHC-8 [27]. Although newer generations of the Dash-8 use a combination of a Pratt & Whitney PW150A and Dowty Propeller R408/6-123-F/17, this significantly reduces the relative difference between the two aircraft and increases the margin to the noise limits.

Similar effects take place for Concept B8. While the number of propellers is unchanged relative to the two present on the reference Twin Otter, the decrease in diameter results in a lower tip Mach number. The noise benefits due to the reduction in tip speed and increase in number of blades do not outweigh the increased contribution of the loading noise source (both lift and drag components) due to the increased thrust requirement.

The design, however, could benefit from more closely replicating the design choices of the similarly sized, currently certified Jetstream 31. Despite being a larger and heavier aircraft, the Jetstream manages to have lower certification levels relative to the DHC-6 [27], while also using two propellers for thrust generation.

Due to minimal changes in design and operation between the ATR72-600 and Concept E1 propellers, noise variation is caused by changes in thrust requirements. Further investigation of the sources associated with direct hydrogen combustion is required. These sources may be direct results of the combustion process or indirect due to the introduction of cooling ducts and vents [34], causing additional cavities and/or duct-related acoustic phenomena.

VII. Discussion

Overall, the NPD calculation is a process with many intermediate steps between the generation of noise at the individual source level and the reception of the total aircraft noise levels (instantaneous and exposure), after propagation, at any observer location. Replication of experimental results depends on the methods and models employed at each step of that procedure, as well as knowledge of the experimental setup/strategy, conditions, and processing techniques that result in comparison data.

A. Whole Aircraft Noise Model Uncertainty

The main sources of error are due to two main components of the computational method for generating NPD curves: i) noise source definition and ii) propagation. Representing an air vehicle/aircraft as a lumped acoustic source requires empirical assumptions about the contribution of each individual source mechanism to the overall sum and the balance between them as a function of aircraft and engine operation. The subsequent propagation of the acoustic signature is heavily influenced by atmospheric effects such as temperature, humidity, and wind direction and magnitude on an average but also local basis. Gradients and fluctuations of these parameters can alter the propagation paths and levels of the initial signal through refraction and scattering effects.

More specifically, three main factors contribute to an erroneous lumped source definition, which then has a knock-on effect on the NPD process. These are i) unaccounted for individual noise source mechanisms, ii) the far-field radiation directivity of individual noise sources and their effect on the overall air vehicle directivity, and iii) the spectral content of individual noise sources and their effect on the overall sound frequency spectrum. In the context of the NPD curve creation, each of these factors can alter the final results, causing under- or overestimation of noise levels at observer locations.

1. *Unaccounted Source Mechanisms*

Although propeller noise is dominated by low-frequency tones that are captured by modeling the steady loading and thickness noise source contributions, it is worth considering the impact of two additional sources: unsteady loading harmonic noise and broadband noise, specifically due to turbulence ingestion.

Beyond propulsion noise sources, airframe noise modeling, especially in the approach condition, is critical. The simplistic implementation of the Fink model, accounting for only variation in airspeed and flap angle deflection through PWL scaling relations, does not take into account changes in the frequency content and directivity of airframe noise.

However, the validation and concept prediction cases did not see any major airframe (if any) design or flight configuration changes between the baseline and predicted aircraft that would require additional deltas. This leads to the conclusion that a possible underprediction of airframe noise is due to the initial source balance estimation rather than errors in the estimation of the deltas.

2. *Directivity*

The interplay of directivity and distance to the observer impacts the location (temporal or spatial, dependent on reference), level, and spectral content of the $L_{A,\max}$ for any single event. These same relations determine the distribution of the acoustic energy during an event duration at any observer location in the 10-dB down window, used for the estimation of exposure metrics such as SEL.

The SAE AIR 1845 procedure uses a "simplified adjustment procedure" to calculate the sound exposure levels L_{AE}, at distances other than the ones the baseline level was calculated/measured at. The adjustment is empirical and is known to cause discrepancies in the levels when the difference in slant distance between the estimation point and the baseline point is large, as the assumption that the effective event duration $D_{AE,d} \propto d^{0.75}$ breaks down. The application of this simplified procedure can be avoided by manually calculating the L_{AE} performing simulated flyover at each slant distance. This is the solution used by Rizzi et al. [14].

In addition, the procedure assumes a constant emission angle for $L_{A,\max}$ for distances greater than 800 m. The calculations suggested for SAE AIR 1845 are done with the presumption that the sound emission angle at the moment of the maximum sound level for the test distance does not change with increased distance.

Because atmospheric–absorption processes greatly lower the high-frequency sound pressure levels at large distances, the assumption of a constant sound emission angle during the time of occurrence of the highest sound level is not necessarily true. As a result, as the distance grows, the relative time at which the maximum sound level occurs may shift.

The implications of an erroneous directivity are beyond the two points made above in the case of sound exposure calculation. As an example, take the extreme case of an axially (parallel to the flight axis) oriented dipole ($D_{\max}$ occurs at $\beta = 0$ and $\beta = pi$) and one perpendicular to that ($D_{\max}$ occurs at $\beta = \pi/2$). In the first case, maximum radiation occurs early and late in the event time history relative to the observer, where the distances are large (and $\rightarrow \infty$ for a flight path of infinite length), whereas minimum radiation occurs at the point of closest approach. The integrated exposure level for a flyover of the dipole would be significantly lower than that of the second case, where maximum radiation occurs at the point of closest approach. This trivial example indicates the effect that is believed to contribute to the error observed in the NPD curves calculated in this section.

3. *Frequency Content*

As with directivity, spectral content is affected by the variation of distance throughout a flyover. In the case of propeller harmonic noise, the majority of the energy is located in the low-frequency BPF and its harmonics. For low slant distances and low tip relative Mach numbers, it is expected that atmospheric absorption will have little impact on the received signal. However, within the framework, there is a tendency to overpredict high-frequency content. This means that, for a given OASPL, energy is shifted to the high frequencies, which are more vulnerable to being attenuated by the atmosphere.

Finally, the dependence of frequency on directivity is worth repeating, as this is a gross assumption within the framework that alters levels received at the observer locations.

4. *NPD Curves*

A discussion is presented on the comparison of numerically calculated NPD curves with measured ones. Large-scale outdoor acoustics campaigns for certification and NPD curve creation purposes are difficult to replicate for the following fundamental reasons: The first pertains to the actual state and conditions of the aircraft and propulsion systems (and therefore the parameters that feed into the individual noise source models) at any given time throughout a measurement event. The discrepancy between flight parameters in real operation and their values defined from reverse engineering or calculating them based on power setting parameters such as rpm (in the case of propellers) presents another source of error relative to outdoor measurements.

Second, performance transient conditions (aircraft and propulsion system) are avoided in the process of NPD curve creation, as steady-state conditions are the targets. The impact of transient conditions on the aeroacoustics is twofold: i) time-dependent driving parameters (due to acceleration or deceleration of rotating machinery, for example), and ii) the influence on noise source breakdown. Obviously, both of these conditions impact the assumptions of the framework.

Finally, all predictions and experimental data should be returned to reference atmospheric conditions. This is standard procedure for the development of NPD curves in order to provide a basis for comparison. Although conditions are typically monitored at standard intervals during the measurement campaign, at the observer location and at the aircraft flyover altitude, variations in atmospheric conditions may still introduce errors in the observed acoustic signal.

B. Limitations

The framework is exposed to limitations due to its dependency on experimental data. Two types of data are required by the framework:

flight NPD curves for a representative baseline aircraft and individual source baseline data. Inherently, therefore, the accuracy of the framework is highly dependent on the quality/relevancy (applicability) of said data, in the absence of which limitations become more pronounced.

Another limitation of an aircraft noise prediction model in the absence of good baseline data is the inability to identify novel (unforeseen) sources of noise. A good baseline data set is necessary to identify the sources of noise, which can then be used to develop appropriate lumped source representations.

As expected, the choice of baseline aircraft is critical to the validity of the linear approximation. Vehicles with no clear reference vehicles will be susceptible to the previous limitation and require a combination of closely working with design teams and engineering judgment based on the expected design and operation to accurately define the lumped source model and iterate appropriately. Validation of such a lumped source model would require full-scale flight test data. However, the framework should be used as a guide for well-understood sources to prevent major noise risks and as a tool that can provide an impact assessment of potential unknown sources of noise.

Beyond conceptual and the early stages of preliminary design, detail changes in design (e.g., propeller blade sweep) and operation are not captured appropriately. Assessment of the impact of detailed design is beyond the scope of the tool, unless the individual source methods are updated to a higher fidelity or semi-empirical models that leverage the models and data of the detailed designs.

Finally, access to actual operational (trajectory and performance) data is limited, confining flight modeling to the straight-level NPD flight procedures, which may not be representative of NPD experimental campaigns. Additionally, operation and performance (total air vehicle and performance) are difficult to extrapolate when in the conceptual design stages. Generally, the NPD process lends itself to cases where the operation of a given aircraft can be broken down into simple segments of constant performance. This is not necessarily the case for all novel aircraft, especially air vehicles in the AAM sector. Such vehicles are characterized by transient phases of flight that require multiple operational modes to describe a single takeoff or landing procedure. Each mode requires a specific definition of possible transient performance data and corresponding complex lumped noise source models. The assumptions regarding the source breakdown are also invalidated, requiring additional sets of data to inform that process.

C. Model Strengths and Suggested Use

Predictions are based on readily available noise and performance data. A detailed definition of design and operation parameters is not required, as the intended use environment within conceptual design does not lend itself to detailed design and high-fidelity data sets. Reduced setup and run time allow for quick iteration and feedback to be provided to design teams. This also allows for parametric studies or Monte Carlo–type simulations when uncertainty exists within the input parameters.

The lumped source model allows for flexibility in the definition of the representative sources and is easily extensible when methods and/or data exist for the calculation of deltas. It provides an insight on how the PWL, directivities, and spectral content of the individual sources combine together to form the total noise signature of the aircraft and how that manifests in operational noise and specifically noise event metrics: instantaneous, $L_{A,\max}$, and exposure SEL, which is not intuitive. When coupled with appropriate data sets, the tool allows for the assessment of changes in operation (e.g., operational weight) for configuration comparisons and changes in design (e.g., propeller diameter) and the relative impact between the two. Additionally, the contributing individual sources are not limited to the ones discussed herein; although not trivial, any source method can be used to produce the required PWL, directivity, and spectral shapes and contribute to the overall lumped source definition. By comparing the relative difference between NPD curve predictions, it is possible to gain a perspective on how changes in individual noise source levels manifest themselves in the context of a whole aircraft, on the ground, and in terms of exposure metrics.

VIII. Conclusions

A framework for computationally generating NPD data for current and concept propeller-powered aircraft was presented in this paper. The framework is a whole-air-vehicle noise prediction tool used to model air vehicles as the sum of individual sources for the estimation of certification and operational noise. This was an update to the original lumped noise source method developed by Synodinos et al. [1] to account for tonal noise sources. A specific method for propeller steady harmonic noise was derived and included in the definition of the lumped source model. This method is an asymptotic approximation to the Hanson frequency domain propeller harmonic noise model [23]. The resulting formulation gives the far-field SPL as a function of the fundamental tone of the acoustic signature and a shape function describing the levels of the harmonics relative to that fundamental. Changes in noise levels between two designs and/or operating conditions are then estimated and combined with a reference baseline case to produce predictions for the new concepts. Finally, NPD curves are generated using the derived noise levels and the implementation of computational steady-level flyovers.

Predictions for current fixed-wing propeller-powered aircraft were used as benchmarks, while predictions for hydrogen-powered propeller concepts were also presented. Two main assumptions were made regarding the description of the lumped source representation of the aircraft as a noise source:

1) The lumped noise source model is composed of two individual sources: propeller harmonic noise and airframe noise. Noise at takeoff is dominated by steady propeller harmonic noise, this being loading (lift and drag) as well as thickness noise sources.

2) The overall aircraft directivity is assumed to be a PWL-weighted average of the individual source directivities.

It allows simple testing of assumptions such as source balance, breakdown, and dominance while capturing all the high-level design variations expected to occur at the preliminary design stage of a propeller-powered aircraft. Finally, it provides guidance on the impact of changes in various design parameters on the individual noise sources they affect and how the whole vehicle's noise signature changes as a result. These calculations may be performed in parallel with the design iteration process and leveraged to provide constructive feedback.

Appendix A: Methodology of Error Analysis

Assuming that the noise level L_p is a function of parameters η_j, where j is an index through the total number of parameters influencing source i, a baseline condition denoted with subscript 0 may be expressed as

$$L_p = f(\eta_{0,j}) = f(\eta_{0,1}, \eta_{0,2}, \ldots, \eta_{0,n}) \tag{A1}$$

After implementing changes in operation and design, the parameters become $\eta_1, \eta_2, \ldots, \eta_n$ where $\eta_j = \eta_{0,j} + \Delta\eta_j$, and the sound levels become

$$L_p = f(\eta_j) = f(\eta_{0,1} + \Delta\eta_1, \ldots, \eta_{0,n} + \Delta\eta_n) \tag{A2}$$

The function f will be used to denote the exact value of the noise function, while g is the linear approximation of f. The SPL of an aircraft of s noise sources may be given by

$$L_{p,0} = 10\log\left(\sum_{i=1}^{s} 10^{L_{p,0,i}/10}\right) \tag{A3}$$

where $L_{p,0,i}$ are the sound pressure levels of the individual incoherent noise sources that make up the total aircraft noise. If changes to parameters η_j are made to the individual sources, as means of implementing technological/operational changes, the new SPL may be written as

$$L_p = 10\log\left(\sum_{i=1}^{s} 10^{[L_{p,0,i}+\Delta L_i(\eta_0+\Delta\eta)]/10}\right) \tag{A4}$$

Each individual noise source i may be expressed as a sum of the baseline value and the changes due to variation to each of the parameters:

$$L_{p,i} = L_{p,0,i} + \sum_{j=1}^{n} \Delta L_{i,j}(\eta_{0,j} \to \eta_{0,j} + \Delta\eta_j) \tag{A5}$$

To estimate the change terms $\Delta L_{i,j}$ for each source with respect to all the parameters influencing it, we take the multivariable Taylor series of the function $L_{p,i}$ at the point of the baseline aircraft. Taking into account the logarithmic nature of the function L_p, for the typical applications, the baseline levels are already reasonably high, meaning that the argument of the logarithm is $p_{\text{rms}}^2/p_{\text{ref}}^2 \gg 1$. Modifications to the parameters are assumed to be small as incremental improvements to design and operation are expected. Taking these assumptions into account, the single-term linear approximation is assumed, and higher-order terms are neglected. Comparing the single-order Taylor series with Eq. (A5), we have

$$\sum_{j=1}^{n} \Delta L_{i,j}(\eta_{0,j} \to \eta_{0,j} + \Delta\eta_j) = \sum_{j=1}^{n} \frac{\partial L_{p,i}(\eta_{0,1},\ldots,\eta_{0,n})}{\partial\eta_j}(\eta_j - \eta_{0,j}) \tag{A6}$$

or the change to a single individual source is

$$\Delta L_i = \sum_{j=1}^{n} \frac{\partial L_{p,i}}{\partial\eta_j}\Delta\eta_j \tag{A7}$$

In the case of the Hanson propeller harmonic noise model, the baseline case may be written as

$$L_{p,0} = 10\log\left(\sum_{m=1}^{\infty} 10^{L_{0,m}/10}\right) \tag{A8}$$

where $L_{0,m}$ are the SPLs of the individual harmonics tones. For added modularity to the proposed model, the levels are referenced to the fundamental tone. This is the method implemented in Eqs. (3) and (4). Equation (4) is the result of applying changes $\Delta\eta_j$ to the baseline point.

The new level of the fundamental tone and the new shape function are therefore given by

$$L_{f_1} = L_{f_1,0} + \Delta L_{f_1}(\eta_j \to \eta_j + \Delta\eta_j) \tag{A9}$$

and

$$F_1(m) = F_{1,0}(m) + \Delta F_1(m, \eta_j \to \eta_j + \Delta\eta_j) \tag{A10}$$

To estimate ΔL_{f_1} and ΔF_1, the linear approximation in Eq. (A7) is employed. The changes are expressed as

$$\Delta L_{f_1} = \sum_{j=1}^{n} \frac{\partial L_{f_1}(\eta_{0,1},\ldots,\eta_{0,n})}{\partial\eta_j}(\eta_j - \eta_{0,j}) \tag{A11}$$

and

$$\Delta F_1(m) = \Delta F_1\left(\frac{f}{f_1}\right) = \sum_{j=1}^{n} \frac{\partial F_1(m,\eta_{0,1},\ldots,\eta_{0,n})}{\partial\eta_j}(\eta_j - \eta_{0,j}) \tag{A12}$$

Equations (A11) and (A12) form the generalized versions of the previously derived Eqs. (19) and (21).

To calculate the error caused by the linear approximation, the partial derivatives are calculated using a numerical central differencing scheme using six points. Illustrations of the function and the tangents calculated by the numerical derivative for four different parameters may be seen in Fig. B1. The tangent of the function is calculated at the baseline point. The difference between the two curves is shown as the error in Fig. 4.

Appendix B: Computational Procedure for Developing Noise–Power–Distance Curves

The contents of this appendix aim to extend the framework presented by Synodinos et al. [1] for the generation of NPD curves from the derived change in overall PWL (ΔPWL) and spectral shape of the propeller harmonic sources.

The procedure involves the standard, steady-level flyover of the aircraft directly over a stationary observer, as depicted in Fig. B2. In addition, the NPD curves of the baseline scenario used to compute the ΔPWL are required. The baseline NPD data are backpropagated to the source PWL, where the estimated ΔPWL for the novel scenario is added. The changes to the 1/3rd octave band spectra are also accounted for at this lumped source stage. Once the adjusted spectra have been acquired, spherical spreading, A-weightings, and atmospheric attenuation are accounted for, and thus OASPL NPD levels at all 10 standard slant distances are generated.

The standard SAE AIR1845 [3] computational step is then used to acquire noise exposure NPD curves in SEL or EPNL metrics. For an in-depth description, the reader is encouraged to follow the procedure described in [1,2] along with the SAE AIR1845 [3].

The procedure is outlined in the form of bullet points where differences between propeller aircraft and conventional turbofan aircraft are specified.

1) A baseline scenario is chosen with an experimentally measured $L_{A,\max}$ NPD level at distance d and polar angle θ.

2) The measured $L_{A,\max}$ is backpropagated to the source. This means the removal of the A-weighting, the removal of the atmospheric attenuation correction, and the correction for spherical spreading. The decomposition into 1/3rd octave band spectra was done with knowledge of the baseline shape F_1 and the methodology presented in [20].

3) A lumped noise source is appropriately defined to represent the aircraft of interest. This "total" noise source is made up of the dominant individual noise sources that contribute to the overall noise emission of the aircraft.

4) The change in SPL ($\Delta L_p(d, j)$) is calculated using the changes in individual noise source levels. The changes in individual sources are calculated using appropriate noise prediction methods. In the case of propeller harmonic noise source, the change in noise is calculated with the procedure described in the previous section.

5) $\Delta L_p(d, j)$ is added to the baseline NPD level to yield the aircraft L_p corresponding to the new scenario at the same power setting, and slant distance. In the case of the propeller sources, the new SPL is calculated using Eq. (4), taking into account the change in fundamental frequency level and spectra shape.

6) Changes ΔL_p reflecting changes in power settings of the modified scenario are calculated using the same procedure, only using the L_p corresponding to the new scenario as a baseline level.

7) The levels at the remaining engine power settings at the same distance d are obtained by adding the noise level variation ΔL_p resulting from changing the engine power to the first level $L_p(d, j)$ of the modified scenario.

8) The SAE AIR1845 computational step is then used to propagate the levels at distance d and the remaining NPD distances. This step accounts for atmospheric attenuation corrections.

9) Finally, A-weighting is reapplied, and the 1/3rd spectra are logarithmically summed to get the total $L_{A,\max}$ of the modified scenario.

At this point, $L_{A,\max}$ NPD curves have been derived. The next few steps summarize the procedure for the development of L_{AE} NPD relationship.

1) Using the estimates of the total sound power emitted (at power setting j) of the modified scenario and the directivity characteristics of the aircraft, computational flyover is performed at an altitude equal

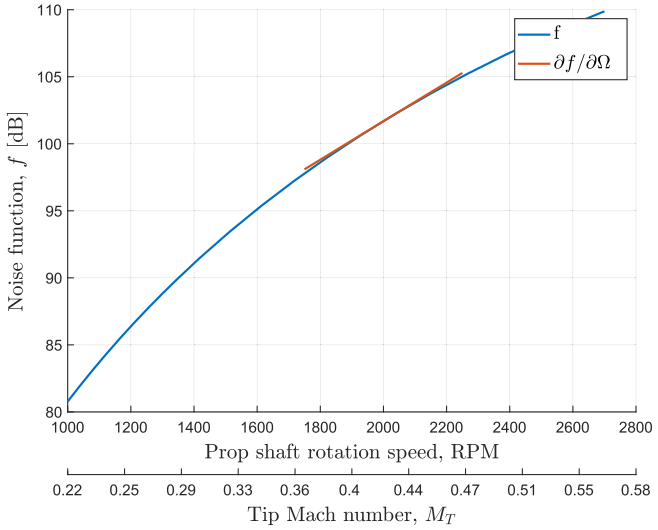

a) Variation of *f* as a function of propeller rotational speed

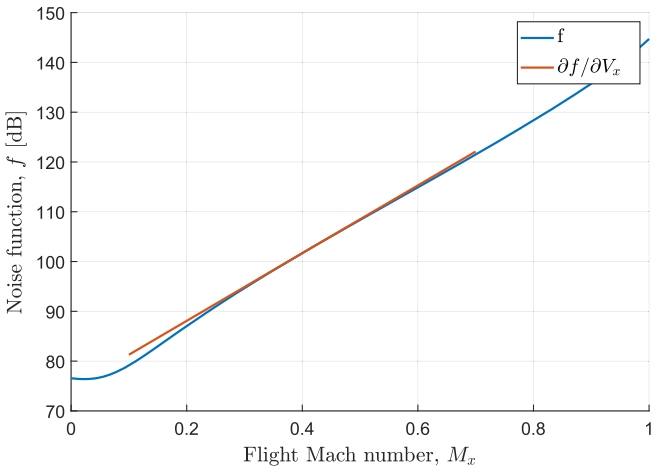

b) Variation of *f* as a function of flight mach number

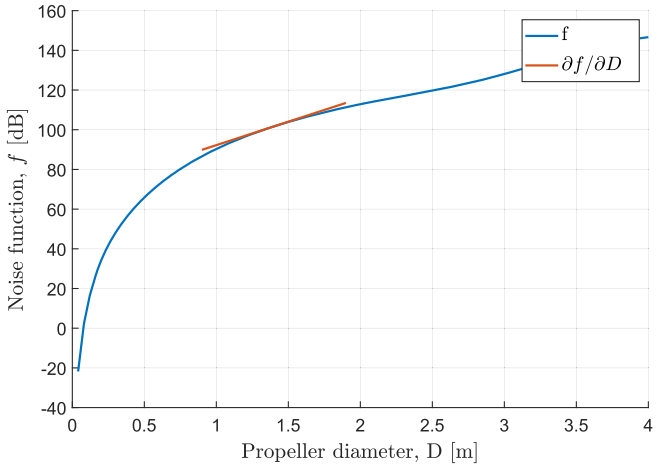

c) Variation of *f* as a function of propeller diameter

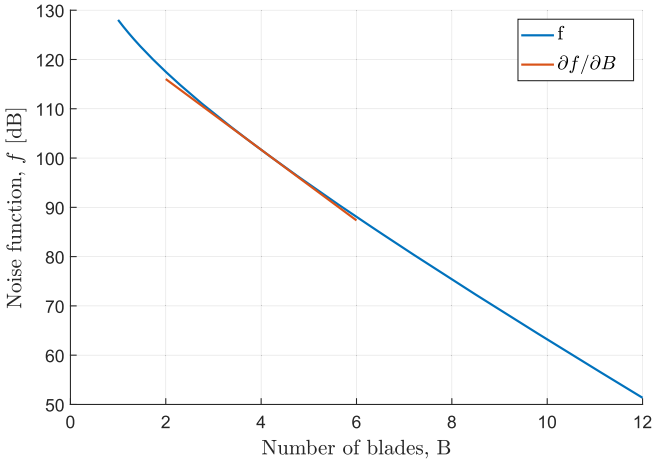

d) Variation of *f* as a function of propeller number of blades

Fig. B1 First-order Taylor series (linear) approximation of the Hanson model. The tangent line slopes are calculated using the partial derivative w.r.t each parameter $\Delta\eta_j$. Baseline parameters shown are $D = 1.4$ m, $B = 4$, $M_x = 0.4$, and $N = 2000$ rpm.

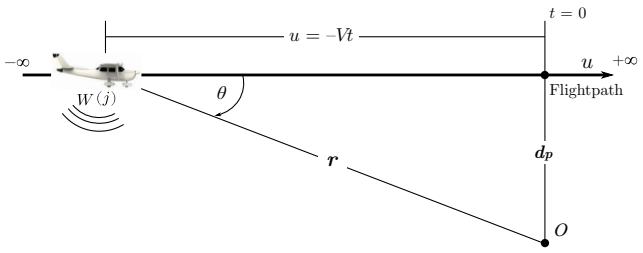

Fig. B2 Geometrical setup during steady-level flyover operation between the moving aircraft and the stationary observer.

to distance d, and L_{AE} is calculated at an observer point directly under the flight path by integration.

2) Using L_{AE} and the previously derived $L_{A,\max}$ NPD curve (at power setting j), L_{AE} is calculated at the remaining NPD slant distances.

3) This procedure is carried out for every power setting of interest.

Appendix C: Concept Aircraft Design Parameters

This appendix is devoted to presenting the design characteristics of the three concept aircraft for which NPD curves are presented in Sec. VI. The concepts are code-named as B5, B8, and E1 as a result of the data management during the design stages, with no particular correlation to the individual design. It is worth noting that all concepts are still in the preliminary stage of design, and the purpose of this study is not to optimize these designs; it is, however, to showcase the capability of the proposed noise framework to work in parallel with the design teams and perform acoustic evaluation provided with the limited data and resources at the early design stages.

C.1. Concept B5

Concept B5 is a clean-sheet high-wing propeller design based on the specifications of the de Havilland Canada DHC-6 Twin Otter. The design is powered by four propellers driven by electric motors. Energy is stored in the form of gaseous hydrogen (H_2) and converted to useful electrical power through the use of fuel cells. Pressurized spherical tanks are used for the storage of the H_2 and are located at the rear of the fuselage. The general dimensions of the aircraft are dictated by the volume constraints that accompany gaseous H_2. A summary of the performance and operational characteristics of the concept may be seen in Table C1.

C.2. Concept B8

Concept B8 is a clean-sheet high-wing propeller design also based on the specifications of the de Havilland Canada DHC-6 Twin Otter. The design features two propellers driven by electric motors. Energy

Table C1 NAPKIN aircraft concept design and performance characteristics required for NPD calculation

	Baseline	Concept		Baseline	Concept
Parameter	DHC-6	B5	B8	ATR72-600	E1
MTOW, kg	5,670	7,376	10,000	22,800	19,600
MLW, kg	5,579	7,376	— —	22,350	18,750
Max static thrust, kN per engine	8.483	5.078	14.90154	53.379	— —
Max takeoff one engine inoperative, kN	— —	— —	— —	— —	21.4
Takeoff thrust, kN per engine	7.979	3.2	9.697125	— —	19.5
Landing thrust, kN per engine	— —	— —	2.491004	— —	3.6
Takeoff airspeed, m/s	38	37.86	61	62	59.7
Landing airspeed, m/s	38.84	39.77	70	61	58.1
Climb angle, °	10	4.5	8.6	6	6.5
Approach angle, °	3	3	3	3	5.5
Number of propellers	2	4	2	2	2
Shaft power, kW per motor	462.3	170	1,000	2,475	2,030
Number of blades	3	3	5	6	6
Propeller diameter, m	2.6	2.6	2.2	3.93	3.96
Propeller rpm (at TO)	2,110	2,016	2,200	1,200	1,200
Propeller rpm (at APP)	1,650	1,562	2,200	1,200	1,200
Propeller rpm (at LAND)	2,110	2,000	2,200	1,200	1,200
Average blade chord, mm	— —	— —	— —	— —	— —
Blade average thickness, m	— —	— —	— —	— —	— —
Propeller efficiency (at TO)	0.59	0.52	0.75	— —	— —
Propeller efficiency (at APP)	0.8	0.8	0.75	— —	— —
Propeller efficiency (at LAND)	0.6	0.66	0.75	— —	— —
PAX (82 kg/pax)	19	19	19	72	48
Max payload with fuel, kg	1,375	1,558	2,218	7,550	4,560
Range, km	750	795	550	1,403.82	1,963
Flap angle takeoff, °	10	10	10	15	15
Flap angle approach, °	10	10	10	— —	— —
Flap angle landing, °	37.5	20	35	— —	— —

TO, Max Takeoff; APP, Approach (intercepted approach flightpath/glide-scope); LAND, Landing/final approach.

is stored in the form of liquid hydrogen (LH_2) and converted to useful electrical power through the use of fuel cells. The aircraft and the propulsion system have been designed to comply with the Certification Specifications for Large Aeroplanes (CS-25). A summary of the performance and operational characteristics of the concept may also be seen in Table C1.

C.3. Concept E1

Finally, Concept E1 is a high-wing propeller design based on the specifications of the ATR72-600. As the reference aircraft, the concept features two propellers. The conventional gas turbine turboprops are replaced with a novel liquid hydrogen turboprop propulsion system. The reference aircraft structure mass and airframe dimensions have been kept constant. Tanks are used for the storage of the LH_2 and are located at the rear of the fuselage. A summary of the performance and operational characteristics of the concept may also be seen in Table C.1.

Acknowledgments

This work was supported by the UK Research and Innovation project New Aviation, Propulsion, Knowledge and Innovation Network (NAPKIN) consortium. We thank Cranfield Aerospace Solutions (CAeS) for providing data for Concept aircraft B5 and, in particular, Robert Jones for his comments on the manuscript. We would also like to thank GKN Aerospace Services and Rolls-Royce plc for providing data for Concept aircraft B8 and E1, respectively. This work was funded by the UK's innovation agency, Innovate UK (TSB Project NAPKIN grant no. 1466348). Antonio J. Torija would like to acknowledge the funding provided by Innovate UK for the InCEPTion project (ref 73692) and by the UK Engineering and Physical Sciences Research Council for the DroneNoise project (ref. EP/V031848/1).

References

[1] Synodinos, A. P., Self, R. H., and Torija, A. J., "Framework for Predicting Noise–Power–Distance Curves for Novel Aircraft Designs," *Journal of Aircraft*, Vol. 55, No. 2, 2018, pp. 781–791. https://doi.org/10.2514/1.C034466

[2] "Report on Standard Method of Computing Noise Contours Around Civil Airports, Vol. 2: Technical Guide," Tech. Rept. ECAC.CEAC DOC. 29, 4th ed., European Civil Aviation Conference (ECAC), Dec. 2005.

[3] A-21 Aircraft Noise Measurement Aviation Emission Modeling, "Procedure for the Calculation of Airplane Noise in the Vicinity of Airports," Aug. 2012, https://www.sae.org/standards/content/air1845a/. https://doi.org/10.4271/AIR1845A

[4] A-21 Aircraft Noise Measurement Aviation Emission Modeling, "Method for Predicting Lateral Attenuation of Airplane Noise," Oct. 2019, https://www.sae.org/standards/content/air5662/. https://doi.org/10.4271/AIR5662

[5] A-21 Aircraft Noise Measurement Aviation Emission Modeling, "Standard Values of Atmospheric Absorption as a Function of Temperature and Humidity," Dec. 2012, https://www.sae.org/standards/content/arp866b/. https://doi.org/10.4271/ARP866B

[6] Koopmann, J., Hansen, A., Hwang, S., Ahearn, M., and Solman, G., "Aviation Environmental Design Tool (AEDT) Version 2c Technical Manual," Tech. Rept. DOT-VNTSC-FAA-16-17, Federal Aviation Administration (FAA), July 2016.

[7] "Integrated Aircraft Noise and Emissions Modelling Platform," EUROCONTROL, 2022, https://www.eurocontrol.int/platform/integrated-aircraft-noise-and-emissions-modelling-platform.

[8] Torija, A. J., Self, R. H., and Flindell, I. H., "A Model for the Rapid Assessment of the Impact of Aviation Noise Near Airports," *Journal of the Acoustical Society of America*, Vol. 141, No. 2, 2017, pp. 981–995. https://doi.org/10.1121/1.4976053

[9] Lopes, L., and Burley, C., "Design of the Next Generation Aircraft Noise Prediction Program: ANOPP2," *17th AIAA/CEAS Aeroacoustics Conference*, AIAA Paper 2011-2854, 2011. https://doi.org/10.2514/6.2011-2854

[10] Bertsch, L., and Krammer, P., "PANAM-A Noise Prediction Tool for Conceptual Aircraft Design," 2008, https://elib.dlr.de/54207/.

[11] Bertsch, L., Guerin, S., Looye, G., and Pott-Pollenske, M., "The Parametric Aircraft Noise Analysis Module—Status Overview and Recent Applications," *17th AIAA/CEAS Aeroacoustics Conference*, AIAA Paper 2011-2855, 2011. https://doi.org/10.2514/6.2011-2855

[12] Rizzi, S. A., Palumbo, D. L., Hardwick, J. R., and Christian, A., "Recent Advances in Aircraft Source Noise Synthesis," *Journal of the Acoustical*

Society of America, Vol. 136, No. 4, 2014, pp. 2285–2286. https://doi.org/10.1121/1.4900264

[13] Rizzi, S., and Rafaelof, M., "Community Noise Assessment of Urban Air Mobility Vehicle Operations Using the FAA Aviation Environmental Design Tool," *INTER-NOISE and NOISE-CON Congress and Conference Proceedings*, Vol. 263, No. 6, 2021, pp. 450–461, https://www.ingentaconnect.com/content/ince/incecp/2021/00000263/00000006/art00045.

[14] Rizzi, S. A., Letica, S. J., Boyd, D. D., and Lopes, L. V., "Prediction-Based Approaches for Generation of Noise-Power-Distance Data with Application to Urban Air Mobility Vehicles," *28th AIAA/CEAS Aeroacoustics 2022 Conference*, AIAA Paper 2022-2839, 2022. https://doi.org/10.2514/6.2022-2839

[15] Rizzi, S. A., and Rafaelof, M., "Second Generation UAM Community Noise Assessment Using the FAA Aviation Environmental Design Tool," *AIAA Scitech 2022 Forum*, AIAA Paper 2022-2167, 2022. https://doi.org/10.2514/6.2022-2167

[16] Li, J., Zheng, Y., Rafaelof, M., Ng, H. K., and Rizzi, S. A., "AIRNOISEUAM: An Urban Air Mobility Noise-Exposure Prediction Tool," *INTER-NOISE and NOISE-CON Congress and Conference Proceedings*, Vol. 263, No. 6, 2021, pp. 474–485, https://www.ingentaconnect.com/content/ince/incecp/2021/00000263/00000006/art00047. https://doi.org/10.3397/IN-2021-1488

[17] Mavris, D., Perullo, C., and Kirby, M., "Project 043 Noise Power Distance Re-Evaluation," Tech. Rept., Partnership for AiR Transportation Noise and Emissions Reduction, 2019.

[18] "Doc 9911, Recomended Method for Computing Noise Contours Around Airports, Second Edition," Tech. Rept., International Civil Aviation Organization, 2018.

[19] Ollerhead, J., "The CAA Aircraft Noise Contour Model: ANCON Version 1," Tech. Rept. DORA 9120, Civil Aviation Authority, Jan. 1992.

[20] Synodinos, A. P., "A New Framework for Estimating Noise Impact of Novel Aircraft," Ph.D. Thesis, Univ. of Southampton, 2017, https://eprints.soton.ac.uk/416509/.

[21] "Aircraft Noise and Performance (ANP) Database v2.1," EUROCONTROL, 2016, http://www.aircraftnoisemodel.org.

[22] Filippone, A., "Turboprop Aircraft Noise: Advancements and Comparison with Flyover Data," *Aeronautical Journal (New Series)*, Vol. 119 No. 1215, 2015, pp. 565–589. https://doi.org/10.1017/S0001924000010691

[23] Hanson, D. B., "Helicoidal Surface Theory for Harmonic Noise of Propellers in the Far Field," *AIAA Journal*, Vol. 18, No. 10, 1980, pp. 1213–1220. https://doi.org/10.2514/3.50873

[24] Hanson, D., and Fink, M., "The Importance of Quadrupole Sources in Prediction of Transonic Tip Speed Propeller Noise," *Journal of Sound and Vibration*, Vol. 62, No. 1, 1979, pp. 19–38, https://www.sciencedirect.com/science/article/pii/0022460X79905546. https://doi.org/10.1016/0022-460X(79)90554-6

[25] Hubbard, H. H., "Aeroacoustics of Flight Vehicles: Theory and Practice: Volume 1: Noise Sources," Tech. Rept., NASA Langley Research Center, Hampton, VA, 1991.

[26] "Type Certificate Data Sheets (TCDS)," European Aviation Safety Agency, 2023, https://www.easa.europa.eu/document-library/type-certificates.

[27] "Type Certificate Data Sheets for Noise (TCDSN)," European Aviation Safety Agency, 2023, https://www.easa.europa.eu/document-library/type-certificates/tcdsn.

[28] "Annex 16 to the Convention on International Civil Aviation: Environmental Protection, Volume I Aircraft Noise," Tech. Rept., International Civil Aviation Organization, July 2017.

[29] Koopmann, J., Hansen, A., Hwang, S., Ahearn, M., and Solman, G., "The CAA Aircraft Noise Contour Model: ANCON Version 1," Tech. Rept. DOT-VNTSC-FAA-16-17, Federal Aviation Administration, July 2016.

[30] "Project NAPKIN New Aviation, Propulsion, Knowledge and Innovation Network: Making Zero-Carbon Emission Flight a Reality in the UK Final Report," Tech. Rept., UK Research and Innovation, 2022, https://www.heathrow.com/company/about-heathrow/future-flight-challenge/napkin.

[31] Kumasaka, H. A., Martinez, M. M., and Weir, D. S., "Definition of 1992 Technology Aircraft Noise Levels and the Methodology for Assessing Airplane Noise Impact of Component Noise Reduction Concepts," NASA CR-198298, 1996.

[32] Fink, M. R., "Noise Component Method for Airframe Noise," *Journal of Aircraft*, Vol. 16, No. 10, 1979, pp. 659–665. https://doi.org/10.2514/3.58586

[33] "ATR 72-600 Aircraft," ATR-Aircraft, Oct. 2020, https://www.atr-aircraft.com/our-aircraft/atr-72-600/.

[34] Sampath, P., and Shum, F., "Combustion Performance of Hydrogen in a Small Gas Turbine Combustor," *International Journal of Hydrogen Energy*, Vol. 10, No. 12, 1985, pp. 829–837, https://www.sciencedirect.com/science/article/pii/0360319985901727. https://doi.org/10.1016/0360-3199(85)90172-7

https://dspace.org/

Toward estimating noise–power–distance curves for propeller-powered zero-emission hydrogen aircraft

Amargianitakis, Daniel C.; Self, Rodney; Torija, Antonio J.; Proenca, Anderson R.; Synodinos, Athanasios P.

2024-03-01
American Institute of Aeronautics and Astronautics (AIAA)
https://doi.org/10.2514/1.C037194
Amargianitakis DC, Self RH, Torija AJ, et al., (2024) Toward estimating noise–power–distance curves for propeller-powered zero-emission hydrogen aircraft. Journal of Aircraft, Volume 61, Issue 2, March 2024, pp. 485-502

Downloaded from a DSpace repository. https://dspace.org/